Journal of Molecular Liquids 264 (2018) 150–164

Contents lists available at ScienceDirect

Journal of Molecular Liquids

journal homepage: www.elsevier.com/locate/molliq

Bicanonical ensemble Monte Carlo simulation of water condensation in the field of crystal lattice defects

S.V. Shevkunov [a,*], Jayant K. Singh [b]

[a] Peter the Great St. Petersburg Polytechnic University, St. Petersburg, Polytekhnicheskaya Street, 29, 195251, Russia
[b] Department of Chemical Engineering, Indian Institute of Technology Kanpur, Kanpur 208016, India

ARTICLE INFO

Article history:
Received 4 March 2018
Received in revised form 17 April 2018
Accepted 2 May 2018
Available online 18 May 2018

Keywords:
Monte Carlo simulation
Condensation
Liquid film
Contact layer
Molecular order
Free energy

ABSTRACT

The free energy, formation work and entropy dependences for water condensate formed from the vapor over the defect-free and containing surface defects basal face of β-AgI crystal at initial stage of condensation at temperatures of 260 K and 400 K are calculated using the bicanonical statistical ensemble method, with Ewald summation for long-range electrostatic and polarization interactions with the substrate. The effect of surface defects in form of rectangular "towers" as a part of regular structure on the stability of condensed phase embryos is investigated. In contrast to small-scale structures, relatively larger coarse-grained nanostructure of crystal surface demonstrates an unconditional advantage in the ability to stimulate condensation compared to defect-free surface. The formation of condensed phase embryos on the surface with multiple defects begins at vapor pressures 5–6 orders of magnitude lower than that on corresponding defect-free surface, and this effect is resistant to temperature variations. The condensate on the surface of the crystal is thermodynamically stable, both on defect-free and nanostructured surfaces, with the exception of short initial stage of the monomolecular film on the defect-free surface.

© 2018 Elsevier B.V. All rights reserved.

1. Introduction

Heterogeneous nucleation of vapor is the main instrument for controlling the precipitation in the atmosphere and influencing local climate [1]. Silver iodide (AgI) in the form of an aerosol is found to be the most active, though rather expensive, agent of water vapor nucleation. The aerosol is prepared by the combustion of suspension of macroscopic crystalline AgI particles in acetone, by shooting from special pyrocartridges attached to the fuselages of aircrafts, or from nozzles of special meteorological rockets. After the sublimation of AgI in high-temperature flame, the silver iodide condenses into crystalline aerosol particles, which serve as nucleation centers for water vapor in the atmosphere. High-temperature processing of AgI suspension is accompanied by a formation of AgI aerosol particles of different shape and sizes so that the surface of the particles can have different surface topography depending on the parameters of the preparation (the temperature, pressure, heating and cooling rates, the AgI vapor density etc.). Nanostructures in form of numerous surface defects can drastically influence the activity of the particles as nucleation centers.

In the last decades, considerable efforts have been directed to computer simulation studies of molecular mechanisms of water condensation on various defect-free crystalline surfaces [2–13] including AgI [14,15,16–18]. Much less work has been reported on surfaces containing single defects and nanostructured surfaces. Small sizes of crystal lattice defects, which are comparable with the radius of intermolecular correlations in liquids, do not allow the application of continuous medium as well as mean field and other approximations that do not take into account consistently the discrete molecular nature of liquids. Computer simulations represent here a most reliable source of information both of fundamental character and related to the surfaces with specific crystal structure.

A distinctive feature of water microcondensation on defect-free surfaces is its layer-by-layer mechanism which can be observed on some crystal substrates. The formation of the first molecular bilayer represents here the most important stage which determines further development of the process [19]. At the same time, the cohesion with the contact bilayer is not a single important factor. It was pointed out in [20] that changes induced by the substrate away from the interface might play an important role in the nucleation mechanism. Orientation order in the first layer at the contact of the liquid with the substrate is essentially important for the growth of next layers and condensed bulk phase as a whole [21]. The first layer of water molecules adjacent to the metal Pt(111) surface was found in [22] to display solid-like properties. The next two layers displayed ordering similar to ice-I. The structure and dynamics of water outside these layers were found to be bulk-like.

* Corresponding author.
E-mail addresses: shevk54@mail.ru (S.V. Shevkunov), jayantks@iitk.ac.in (J.K. Singh).

https://doi.org/10.1016/j.molliq.2018.05.004
0167-7322/© 2018 Elsevier B.V. All rights reserved.

There are only a limited number of investigations performed for water on nanostructured surfaces. In these conditions, the data obtained for the model fluids [23] including the system of Lennard-Jones (LJ) liquids [24] represent here certain compensation. Computer simulation studies for nanoscopic pores [25–28] allowed observing most general regularities accompanying the contact of liquid phase with solid surfaces containing nanoscopic structural elements [29,30]. Multiple defects localized on the surface at the distances compared to the length of intermolecular correlations make the substrate rough and can destroy molecular order in the first molecular layers completely. The LJ droplets on smooth and molecularly rough surfaces consisting of LJ particles were simulated in [31]. The roughness of the substrate was prepared by creating nanoscopic grooves. Wetting was analyzed in terms of contact angles. Despite continuum medium approximation arguments laying in the basis of Wenzel's law [32] which suggest that roughness must always amplify wetting, nanoscopic roughness in [31,33] was found to deteriorate wetting both for strongly and weakly wettable surfaces. Computer simulations of LJ droplets on flat and pillar surfaces in [34] showed that the contact angle increases with the pillar size. In addition to equilibrium state, a long-living metastable state of the droplets was observed which is characterized by incomplete penetration of the liquid into hollows between the pillars. Obviously, wetting properties of roughness are in strong dependence of its characteristic size, and roughness of nanoscopic scales exhibits qualitatively different properties in comparison with macroscopic one.

Nanostructured surfaces can display essentially different properties in interaction with liquid water in comparison with flat, defect-free ones [35,36]. It was found that the existence of a defect enhances the water molecule–and cluster–silica surface interactions, but has little effect on water thin film–silica surface interaction [37]. The origin of the weakening effect on the film–surface cohesion is the collective hydrogen bonding that imposes compromise positions of water molecules with respect to surface. This can qualitatively change the mechanism of nucleation as such. Closely located defects can produce in the contact layer collective effects which are able to speed up or slow down the growth of ice from liquid water. Thus, the roughness can have positive or negative effect on the nucleation. In [38], it was found that atomically flat carbon surfaces in contact with liquid water promote heterogeneous nucleation of ice, while molecularly rough surfaces do not.

Density function theory calculations for water molecules at step edges on rutile $TiO_2(110)$ [39,40] and anatase $TiO_2(101)$ [41–44] substrates showed higher ability of steps to hold water molecules in comparison with ideal surfaces. The calculations are done for a single water molecule in different positions close to the surface. The higher activity of steps was explained by the action of undercoordinated Ti atoms. A dramatic enhancement of adsorption properties with respect to water due to the presence of steps is also confirmed in laboratory experiments with $BaF_2(111)$ surface [45].

Molecular dynamics simulations of the deposition of model water molecules on the substrate with the structure close to the one of platinum crystal lattice with roughness composed of periodic parallel grooves [46] showed that the nucleation behavior of the supercooled water is significantly sensitive to the width of the grooves. This dependence is not monotonous: when the width of the groove matches well with the specific lengths of the ice crystal structure, the nucleation accelerates, if not, the nucleation rate is even smaller than that on the defect-free surface. A complicated character of the dependence of wettability in terms of contact angle on characteristic sizes of roughness elements is confirmed in [47]. One can differ two states of droplets on nanostructured surfaces – with incomplete penetration of a liquid into the gaps between roughness elements (Cassie-Baxter state) [48] and complete contact with the surface including the bottom of nanoscopic hollows (Wenzel state) [49]. The differences in the mechanism of adhesion to the surface in these two cases show themselves also in kinetic properties of the condensate. In particular, the droplets in Cassie-Baxter state have high mobility in their movement along the surface, do not leave traces and show a pronounced tendency to merge into large drops. This phenomenon is used by biological objects to provide strong water-repellent properties of the surfaces [50].

Nucleation of ice on water-ice interface is accelerated by a transverse local electric field that can be treated as simplest model of nanoscopic defect. Field bands exceeding a minimum size of 0.15 nm thick and 0.35 nm wide catalyze ice nucleation just as efficiently as full surface fields [51].

In general, computer studies of the interaction of water with crystal surfaces made it possible to reveal a number of regularities of a fundamental nature, the main of which are the existence of two nucleation scenarios, namely, the drop and layered nucleation, the possibility of forming a monomolecular film with a hydrophobic surface and the dependence of the contact angle on the droplet size. Optimal conditions for the formation of condensed phase nuclei do not imply the strongest adhesion of the first layer of molecules to the surface, but arise at some optimal binding force. The decisive factor here is the orientation molecular order in the contact layer of the liquid.

The situation with nanostructured surfaces is more complicated. Most of the studies of nanostructured surfaces by computer methods are related to ice formation under conditions of surface contact with a supercooled bulk liquid phase. Heterogeneous nucleation in contact with water vapor is much less investigated. The current work is an attempt toward filling this gap.

The present study is focuses mainly on the thermodynamic behavior of nuclei, primarily free energy and the work of formation, as well as their stability. To calculate the free energy at the molecular level, instead of the most popular method of thermodynamic integration [5,21] and less commonly used, but also well-known method of expanded ensembles [52], the bicanonical statistical ensemble method (BSE) is used in this work. This method makes it possible to obtain directly and with minimum expenditures the dependence of the free energy on the size of the nucleus. Until recently, computer simulation was used for studying nanostructures with a characteristic size of its elements of several molecular sizes. In the current work, the formation of condensed water embryos in the field of larger elements of inhomogeneity is simulated - with a cross section size of 13×13 atoms and with the distance between them of the same order of magnitude. With the increase in the spatial dimensions of nanostructure elements, one can expect an increase in collective effects and a more contrasting separation of molecules into those that are accumulated on the upper and lateral parts of the inhomogeneity elements, and also between them, on the supporting surface of the substrate, which will inevitably affect the thermodynamics of nucleation.

2. Interaction model

2.1. Elementary interactions

From considerations of continuity with the model developed in [15], pairwise water-water interaction energy U_{pair}^{w-w} was described in terms of five-center Rahman and Stillinger ST2 interaction potential [19]. The electrostatic interactions of water molecules with the ions of the crystal lattice of the substrate U_{coul}^{l-W} were represented by the sum of the Coulomb interactions of the water molecule point charges q_k contained in the ST2 potential with the ion charges Q_0^n:

$$U_{coul}^{l-W} = \sum_{i,n} \left[\sum_{k=1}^{k=4} \frac{Q_0^n}{| \mathbf{r}_k^i - \mathbf{x}_0^n |} q_k \right], \tag{1}$$

where Q_0^n is point charge of n-th ion, and $\mathbf{x}_0^n$ is its coordinates. Here and below, for brevity, the formulas for electrostatic interactions

are written without a factor $1/4\pi\varepsilon_0$, like in the system of CGS units. The polarization energy of molecules located at points $\mathbf{r}_0^i$ in the lattice ions field is written in the form of the first term of the multipole expansion:

$$U_{pol}^{W-I} = -\frac{1}{2}\alpha_w \sum_i \left[\sum_n \mathbf{E}_n\left(\mathbf{r}_0^i\right)\right]^2, \tag{2}$$

The quantity α_w is water molecule isotropic polarizability, $\mathbf{E}_n(\mathbf{r}_0^i)$ is electric field strength of n-th ion at the point $\mathbf{r}_0^i$, where the i-th molecule is located:

$$\mathbf{E}_n(\mathbf{r}) = \frac{Q_0^n}{\left|\mathbf{r}-\mathbf{x}_0^n\right|^3}\left(\mathbf{r}-\mathbf{x}_0^n\right). \tag{3}$$

The energy of the dipoles induced by the field of the ions on the molecules in the field of other molecules is the sum over all the molecules:

$$U_{ind,perm}^{W-W} = -\sum_j \mathbf{E}^W\left(\mathbf{r}_0^j\right)\mathbf{p}_j^{ind}. \tag{4}$$

The field of the molecules at the point $\mathbf{r}_0^j$, where j-th molecule is located

$$\mathbf{E}^W\left(\mathbf{r}_0^j\right) = \sum_{i\neq j}\sum_{k=1}^{4}\frac{q_k}{\left|\mathbf{r}_0^j-\mathbf{r}_k^i\right|^3}\left(\mathbf{r}_0^j-\mathbf{r}_k^i\right), \tag{5}$$

and the dipole moment of the j-th molecule induced by the field of the lattice ions represents the sum over all the lattice ions: $\mathbf{p}_j^{ind} = \alpha_w \sum_n \mathbf{E}_n(\mathbf{r}_0^j)$.

The energy of interaction between the dipoles induced on the molecules is calculated in form of the first term of multipole expansion:

$$U_{ind,ind}^{W-W} = \sum_{i<j}\left[\frac{\left(\mathbf{p}_i^{ind}\mathbf{p}_j^{ind}\right)}{(r_{ij})^3} - 3\frac{\left(\mathbf{p}_i^{ind}\mathbf{r}_{ij}\right)\left(\mathbf{p}_j^{ind}\mathbf{r}_{ij}\right)}{(r_{ij})^5}\right]. \tag{6}$$

Exchange and dispersion interactions between the ions and the molecules are written in the form of LJ potential

$$U_{LJ}^{I-W} = \sum_n\sum_i 4\varepsilon_0^n\left(\left[\frac{\sigma_n}{R_{ni}}\right]^{12} - \left[\frac{\sigma_n}{R_{ni}}\right]^{6}\right), \tag{7}$$

where $R_{ni} = |\mathbf{r}_0^i - \mathbf{x}_0^n|$ is the distance between the center of the n-th ion and the oxygen atom of the i-th molecule.

The polarization energy of the ions in the field of other ions and of the molecules was obtained as a sum over all the ions:

$$U_{pol}^{I-(WI)} = -\sum_m \frac{\alpha_m^I}{2}\left(\mathbf{E}^I(\mathbf{x}_0^m) + \mathbf{E}^W(\mathbf{x}_0^m)\right)^2, \tag{8}$$

where α_m^I is the polarizability of the m-th ion. The field of all other ions at the point $\mathbf{x}_0^m$, where the center of the m-th ion is located, was calculated according to the formula

$$\mathbf{E}^I(\mathbf{x}) = \sum_{n\neq m}\left[\frac{Q_0^n(\mathbf{x}-\mathbf{x}_0^n)}{\left|\mathbf{x}-\mathbf{x}_0^n\right|^3}\right]. \tag{9}$$

The same values of parameters in the water-ions interaction potential, as in [15], were used: water molecule polarizability $\alpha_w = 1.44\text{Å}^3$, the charge of Ag^+ in AgI crystal lattice $Q_0^+ = 0.6 \times e = +0.96126 \times 10^{-19}\kappa$, water-ion LJ potential parameters $\varepsilon_0^+ = 0.38027 \times 10^{-20} J$, $\sigma_+ = 3.17\text{Å}$, the polarizability of the Ag^+ ion $\alpha_+{}^I = 2.40\text{Å}^3$. The analogous values for the I^- ion are $Q_0^- = -0.6 \times e = -0.96126 \times 10^{-19}\ \kappa$, $\varepsilon_0^- = 0.43241 \times 10^{-20}\ J$, $\sigma_- = 3.34\text{Å}$, and $\alpha_-{}^I = 6.43\text{Å}^3$.

Ag^+ and I^- ions were fixed in accordance with their positions in β-AgI crystal belonging to the $P6_3mc$ spatial symmetry group with lattice parameters a = 4.580 Å and c = 7.494 Å [53,54]. The substrate surface was chosen parallel to the base faces of the unit cell, with Ag^+ ions in surface crystallographic layer. The interactions with the ions of ten crystallographic layers deep into the crystal lattice of the substrate were taken into account explicitly. In the adsorption plane, the summation of long-range electrostatic interactions was carried out by the two-dimensional Ewald method [55]. In addition to direct summation of dispersion interactions within the own periodic cell of each particle, the correction term containing the dispersion interactions with the ions in the periodic cell layers closest to the main periodic cell was taken into account. In particular, the dispersion interactions with lattice ions were summed up within six layers of periodic cells around the own cell of the molecule. Two-dimensional version of Ewald method was applied also for the calculation of polarization energy in the field of lattice ions located beyond the own periodic cells of the molecules (see Appendixes).

Unlike previous computer simulation studies mentioned in the Introduction, in this work, the substrate surface with a much more large-scale relief is simulated. This allows water molecules to more easily penetrate between the nanoscopic elements and makes possible collective effects in the behavior of such molecules. The size of the periodic cell in the adsorption plane in the calculations for the defect-free surface was 126.92 Å × 146.56 Å (32 ions × 32 ions), and for nanostructured surface of 95.194 Å × 109.92 Å (24 ions × 24 ions). In the last case, each periodic cell contained one defect in form of a rectangular 'tower' of six crystallographic layers in height and 13 × 13 ions in cross section, so that the linear size of the defect was about a half of the linear size of periodic cell. The linear dimensions of periodic cell significantly exceed the radius of intermolecular correlations in the adsorbed component.

3. Method

3.1. Calculation of free energy

The calculations of free energy were performed by the modified bicanonical statistical ensemble method (MBSE) [56] which is based on bicanonical statistical ensemble method (BSE) [57,58] successfully tested in solving many chemical physics problems related to liquid phase [59–64]. The MBSE method allows advancing in the calculations at atomic level of absolute values of free energy to systems containing 10^3–10^4 particles and more. In MBSE method, a sequence of transitions between two classes of microstates, with the numbers of molecules n and $n-1$ according to transition probabilities of grand canonical statistical ensemble and with a predetermined for each value of n chemical potential $\tilde{\mu}(n)$ of a virtual thermal bath is generated numerically. The ratio of the probabilities of finding the system in the states with n and $n-1$ molecules in this sequence is

$$\frac{w(n)}{w(n-1)} = \exp\left(-\frac{\Delta\Psi(n,T)-\tilde{\mu}(n)}{k_BT}\right). \tag{10}$$

Here, $\Delta\Psi(n,T) = \Psi_{cond}(n,T) - \Psi_{cond}(n-1,T)$ is a change of $\Psi_{cond}(n,T)$ due to the attachment to the system of n-th molecule. The function $\Psi_{cond}(n,T)$ has the meaning of Helmholtz free energy of the system, $\Psi_{cond}(n,T) = F_{cond}(n,T)$, if the simulation is performed in conditions of a constant volume, and coincides with Gibbs free energy, $\Psi_{cond}(n,T) = G_{cond}(n,T)$ in the case of a constant pressure, that is in the conditions of isobaric-isothermal statistical ensemble.

Left-hand side of Eq. (10) is calculated numerically by Monte Carlo method, and Gibbs/Helmholtz free energy of the attachment can be readily obtained as

$$\Delta G^{th}(n,T,\tilde{\mu}) \equiv \Delta G(n,T) - \tilde{\mu}(n) = -k_B T \ \ln\left(\frac{w(n)}{w(n-1)}\right). \tag{11}$$

The chemical potential of the molecules of the condensate growing on the surface is obtained from Eq. (11), from the very definition of this quantity as the increment of Gibbs free energy:

$$\mu_{cond}(n,T) \equiv \Delta G(n,T) = \Delta G^{th}(n,T,\tilde{\mu}) + \tilde{\mu}(n) \ = -k_B T \ \ln\left(\frac{w(n)}{w(n-1)}\right) + \ \tilde{\mu}^c(n,T) - k_B T \ \ln\left(\frac{8\pi^2}{\sigma}\right) - k_B T \ \ln\left(Z_{tr}^{kin} Z_{rot}^{kin} \mathrm{v}_{ref}\right), \tag{12}$$

where $\tilde{\mu}^c(n,T)$ is translational component of configuration part $\tilde{\mu}^{conf}(n, T) \equiv \tilde{\mu}^c(n,T) - k_B T \ \ln\left(\frac{8\pi^2}{\sigma}\right)$ of the thermal bath's chemical potential $\tilde{\mu}$, and v_{ref} is an arbitrary constant, measured in the units of volume and representing a reference level for the configuration part of chemical potential. $Z_{tr}^{kin} = \left(\frac{h}{\sqrt{2\pi m_w k_B T}}\right)^{-3} = \frac{1}{\Lambda^3}$ and $Z_{rot}^{kin} = \frac{(2k_B T)^{3/2}(I_1 I_2 I_3)^{1/2}\pi^{3/2}}{h^3}$ are the results of integration over the momenta of translational motion and rotational momenta in the partition function of the molecules, h is Plank constant, Λ is De Broglie thermal wavelength, σ is rotation symmetry parameter (is equal to 2 for water), $m_w = 2.992 \times 10^{-26}$ kg is the mass of a water molecule, and $I_1 = 1.024 \times 10^{-47}\,\mathrm{kg} \times \mathrm{m}^2$, $I_2 = 1.921 \times 10^{-47}\,\mathrm{kg} \times \mathrm{m}^2$, $I_3 = 2.947 \times 10^{-47}\,\mathrm{kg} \times \mathrm{m}^2$ are its principle moments of inertia.

Chemical potential $\tilde{\mu}^c(n,T)$ is input parameter of the calculations. There is an optimal value of $\tilde{\mu}^c(n,T)$ which provides minimum statistical error in calculations with finite random samplings. It corresponds to the equality $w(n) = w(n-1)$ and is evaluated numerically by sequential iterations on an initial segment of Markov random process, individually for each value of n.

To obtain free energy of a liquid consisting of N molecules, one should calculate $\mu_{cond}(n,T)$ successively for all the values of n in the range from 1 to N and sum up these quantities numerically: $G_{cond}(N,T) = \sum_{n=1}^{N} \mu_{cond}(n,T)$. So, the successive calculation of $\mu_{cond}(n,T)$ for a series of increasing values of n provides not simply a single value of free energy, but a whole dependence of $G_{cond}(N,T)$ on the size N of the system. This function represents a special interest, since it is the dependence on the size of the system that plays a key role in its thermodynamic stability. In MBSE method, Monte Carlo calculations of $\Delta G^{th}(n,T\tilde{\mu})$ are performed for a certain subset n_i^*, $i = 1, \ldots, K$ of all the values of n from the interval $[1,N]$.

The number of points K and specific values of n_i^* are assigned taking into account expected complexity of the shape of $\mu_{cond}(n,T)$ curve. As a rule, 20–30 control points are enough to reproduce its course with required detail. In special cases, the number of points can be increased to reflect possible irregular dependence on the initial segment of the curve. It is recommended to calculate without gaps, first 7–10 values (with $n_i^* = i$), corresponding to small sizes of the system and to distribute all other point exponentially, $n_i^* \sim \nu^i + const$, with some optimal value of arbitrary constant ν. The configuration parts of chemical potential $\mu_{cond}^{conf}(n_i^*,T) \equiv \mu_{cond}(n_i^*,T) + k_B T \ \ln\left(Z_{tr}^{kin} Z_{rot}^{kin} \mathrm{v}_{ref}\right) = \Delta G^{th}(n_i^*,T,\tilde{\mu}) + \tilde{\mu}^{conf}(n_i^*,T)$ are obtained according to Eq. (11) from the values of $\Delta G^{th}(n_i^*,T,\tilde{\mu})$ calculated by Monte Carlo simulations for each n_i^*, $i = 1, \ldots, K$ and interpolated by cubic splines: a cubic polynomial $f_i(x,T,\tilde{\mu})$ as the function of x with a domain of definition $n_i^* \le x \le n_{i+1}^*$ is constructed for each pair of successive points n_i^* and n_{i+1}^*. According to approximation conditions, the $f_i(x,T,\tilde{\mu})$ curves pass through all the calculated points, $f_i(n_i^*,T,\tilde{\mu}) = \mu_{cond}^{conf}(n_i^*,T)$, $f_i(n_{i+1}^*,T,\tilde{\mu}) = \mu_{cond}^{conf}(n_{i+1}^*,T)$ and are continuously "sewed up" at these points together with their derivatives, $f_i(n_{i+1}^*,T,\tilde{\mu}) = f_{i+1}(n_{i+1}^*,T,\tilde{\mu})$, $\left.\frac{\partial f_i(x,T,\tilde{\mu})}{\partial x}\right|_{x=n_{i+1}^*} = \left.\frac{\partial f_{i+1}(x,T,\tilde{\mu})}{\partial x}\right|_{x=n_{i+1}^*}$. The chemical potential of the molecules for each value of n within the interval $[1,N]$ is obtained from the calculations at control points n_i^* in the following way:

$$\mu_{cond}(n,T) = f_{k(n)}(n,T,\tilde{\mu}) - k_B T \ \ln\left(Z_{tr}^{kin} Z_{rot}^{kin} \mathrm{v}_{ref}\right), \tag{13}$$

and its configuration part $\mu_{cond}(n,T) = f_{k(n)}(n,T,\tilde{\mu})$, the functional dependence $k(n)$ being defined by the condition $n_k^* \le n \ \le n_{k+1}^*$. The free energy at control points n_i^* is calculated by numerical summation over all the points $n = 1, \ldots, n_i^*$, with the step in n equal to unity as

$$G_{cond}(n_i^*,T) = \sum_{n=1}^{n_i^*} \mu_{cond}(n,T) = \sum_{n=1}^{n_i^*} f_{k(n)}(n,T,\tilde{\mu}) - n_i^* k_B T \ \ln\left(Z_{tr}^{kin} Z_{rot}^{kin} \mathrm{v}_{ref}\right), \tag{14}$$

and its configuration part is obtained in the same way as $G_{cond}^{conf}(n_i^*,T) = \sum_{n=1}^{n_i^*} f_{k(n)}(n,T,\tilde{\mu})$.

3.2. Calculation of formation work and entropy

Equilibrium work of condensate formation from the vapor under pressure p was calculated using the formula of ideal gas of rigid rotators for chemical potential of vapor molecules $\mu(p,T)$:

$$A(n_i^*,p,T) = G_{cl}(n_i^*,T) - n_i^* \mu(p,T) = \sum_{n=1}^{n_i^*} f_{k(n)}(n,T,\mu\sim) + n_i^* k_B T \ \ln\left(\frac{8\pi^2}{\sigma}\frac{k_B T}{p\,\mathrm{v}_{ref}}\right) \tag{15}$$

Using Eq. (15) and the condition of the equilibrium between the condensate and the vapor $\frac{\partial A(n,p,T)}{\partial n} = 0$, we can obtain the following:

$$f_{k(n)}(n,T,\tilde{\mu}) = k_B T \ \ln\left(\frac{\sigma}{8\pi^2}\frac{p\,\mathrm{v}_{ref}}{k_B T}\right). \tag{16}$$

As can be seen from Eq. (15), for a given n, variations in vapor pressure do not affect the value of the second derivative:

$$\frac{\partial^2 A(n,p,T)}{\partial n^2} = \frac{\partial f_{k(n)}(n,T,\tilde{\mu})}{\partial n} \tag{17}$$

The sign of which determines the stability of the condensate. Simultaneously with the calculation of free energy, the calculation of internal energy $E_{cond}(n_i^*,T) = U_{cond}(n_i^*,T) + \frac{6}{2} n_i^* k_B T$ as a function of the size n_i^* was executed. The calculation was performed in two ways: by direct averaging the interaction energy of n_i^* molecules and by summation of the energies of attachment reactions $\Delta E(n,T) = U_{cond}(n,T) - U_{cond}(n-1,T)$. The calculations of $U_{cond}(n_i^*,T)$ and $U_{cond}(n_i^* - 1, T)$ have been done simultaneously during a single run by averaging the energy separately over the states with n_i^* and $n_i^* - 1$ molecules, and $\Delta E(n,T)$ was then obtained using the interpolation of $\Delta E(n_i^*,T)$ values by cubic splines. Since in calculations based on finite random samplings the value of $\Delta E(n_i^*,T)$ is obtained as a relatively small difference between two close fluctuating quantities, its relative statistical error grows with increasing size n_i^* as $\sqrt{n_i^*}$ that makes practically impossible the calculations for $n_i^* > 10^3$. In the MBSE method, the calculation of $\Delta E(n_i^*,T)$ for $n_i^* > 30$ is carried out by analytic differentiation of a quadratic polynomial representing as a result of the approximation of last four values of $U_{cond}(n_k^*,T)$, $k = i-3, \ldots, i$ obtained in Monte Carlo calculations. Statistical error of the derivative $\Delta E(n,T) = \frac{\partial U_{cond}(n,T)}{\partial n}$ calculated in this way

decreases with the size of adsorbed component, due to long enough distances between control points, distributed according to exponential law as $(n_i^* - n_{i-1}^*)^{-1} \sim (n_i^*)^{-1}$. Taking into account the variations of statistical error of $U_{cond}(n_k^*, T)$ values ($\propto (n_k^*)^{1/2}$), the resulting relative statistical error of $\Delta E(n_i^*, T)$ behaves approximately as $(n_i^*)^{-1/2}$, i.e. it decreases with the size of the system.

In numerical calculations, the interpolation by cubic splines $g_{k(n)}(n,T)$ of all $\Delta E(n_k^*, T)$ values obtained in Monte Carlo simulations is carried out, with subsequent summation to calculate internal energy $E_{cl}(n_i^*, T) = \sum_{n=1}^{n_i^*} g_{k(n)}(n,T) + \frac{6}{2} n_i^* \, k_B T$ and formation enthalpy $H_f(n_i^*, T) = \sum_{n=1}^{n_i^*} g_{k(n)}(n,T) - n_i^* \, k_B T$. The attachment energy is $\Delta E(n_i^*, T) = g_{k(n_i^*)}(n_i^*, T)$. The entropy was calculated through the difference between internal and Helmholtz free energies $S_{cond}(n_i^*, p, T) = (E_{cond}(n_i^*, p, T) - F_{cond}(n_i^*, p, T))/T$ or between the enthalpy and Gibbs free energy $S_{cond}(n_i^*, p, T) = (H_{cond}(n_i^*, p, T) - G_{cond}(n_i^*, p, T))/T$, where the enthalpy of the system is $H_{cond}(n_i^*, p, T) = E_{cond}(n_i^*, T) + p\, V_0^{cond}$. The enthalpy of attachment reaction in the conditions with a fixed volume V_0^{cond} of the system is equal to $\Delta H(n_i^*, T) = \Delta E(n_i^*, T) - k_B T$, the attachment Gibbs free energy is $\Delta G(n_i^*, p, T) = \mu_{cond}(n_i^*, T) - \mu(p, T)$, and the attachment entropy is $\Delta S(n_i^*, p, T) = (\Delta H(n_i^*, T) - \Delta G(n_i^*, p, T))/T$.

3.3. Simulation algorithm

A random sequence of molecular configurations was generated numerically on the computer, with probabilities of their realization proportional to the equilibrium distribution function of grand canonical statistical ensemble

$$\rho(q_1, \ldots, q_k, k) \propto \frac{1}{k!} \left(Z_{tr}^{kin} Z_{rot}^{kin}\right)^k \exp(\tilde{\mu} k / k_B T - U_n(q_1, \ldots, q_k)/k_B T) \tag{18}$$

with two allowable values of the number of the molecules, $k = n$ and $k = n - 1$, where $U_k(q_1, \ldots, q_k)$ is potential energy, and $q_1, \ldots, q_k$ are the coordinates of the molecules. The sequence of the configurations was obtained by numerical simulation of a single element of the statistical ensemble, the development of which occurs according to the laws of Markov random process. The process was directed by transition probabilities $p(X,Y)$ between the microstates $X = q_1, \ldots, q_n, k_1$ and $Y = q_1', \ldots, q_k', k_2$ which satisfy the detailed balance condition $\rho(X) p(X,Y) = \rho(Y) p(Y,X)$ with equilibrium distribution function $\rho(X)$. One step of the procedure consisted in a trial to go over from a current microstate X into a randomly selected microstate Y. Two types of steps alternated: attempts to bias and rotate one randomly chosen molecule and attempts to remove or add one molecule by placing it at a randomly chosen point in the system. In the execution of the first type steps, all three Euler angles of the molecule to be displaced got random increments uniformly distributed within $(-\delta, +\delta)$ interval with $\delta = 10^\circ$, whereas the increments of the coordinates of the molecular center of mass were uniformly distributed in $(-\Delta, +\Delta)$ interval with $\Delta = 0.15$Å. The transition from a microstate X into a microstate Y was executed with the probability

$$\min\left\{\frac{\sin(\theta_Y)}{\sin(\theta_X)} \exp(-(U_k(Y) - U_k(X))/k_B T),\ 1\right\}, \tag{19}$$

where $U_k(X)$, $U_k(Y)$ are potential energies, and θ_X, θ_Y are Euler angles between the axis of biased molecule and z-axis in the microstates X and Y, correspondingly. The frequency of acceptance of new configurations varied here within the limits of 40–50%. The removal of a randomly selected molecule was executed with the probability

$$p(Y,X) = \frac{1}{n} \min\left\{\frac{n}{V} \exp\left(-\frac{\tilde{\mu}^c - (U_n(Y) - U_{n-1}(X))}{k_B T}\right) \mathrm{v}_{ref},\ 1\right\}. \tag{20}$$

Adding to an elementary configuration volume at a randomly selected point was executed with the probability

$$p(X,Y) = \frac{1}{n} \frac{d\Omega}{8\pi^2/\sigma} \frac{dV}{V} \min\left\{\frac{V}{n} \exp\left(\frac{\tilde{\mu}^c - (U_n(Y) - U_{n-1}(X))}{k_B T}\right) \mathrm{v}_{ref}^{-1},\ 1\right\}. \tag{21}$$

Here, $\Omega = (\alpha, \cos(\theta), \varphi)$, α, θ, φ are Euler angles, and $d\Omega = \sin(\theta)\, d\alpha\, d\theta\, d\varphi$. The new orientation of the molecule was randomly assigned according to the distribution $\propto \sin(\theta_Y)$. The multiplier $1/n$ in Eqs. (20) and (21) is realized, when a specific number of the molecule to be removed or added is randomly assigned, and the multipliers $\frac{d\alpha\, d\theta\, d\varphi}{8\pi^2/\sigma}$ and $\frac{dV}{V}$ manifest themselves, when certain position and orientation of the molecule to be added are randomly selected. The probabilities (20) and (21) satisfy the detailed balance condition which provides the limiting distribution of grand canonical statistical ensemble

$$\frac{p(X,Y)}{p(Y,X)} = \frac{d\Omega}{\left(\frac{8\pi^2}{\sigma}\right)} \frac{dV}{V} \frac{V}{n} \mathrm{v}_{ref}^{-1} \exp\left(\frac{\tilde{\mu}^c - (U_n - U_{n-1})}{k_B T}\right) = \frac{\frac{1}{n!}\left(Z_{tr}^{kin}\right)^n \left(Z_{rot}^{kin}\right)^n \exp([n\tilde{\mu} - U_n]/k_B T)\, d\Omega\ dV}{\frac{1}{(n-1)!}\left(Z_{tr}^{kin}\right)^{n-1} \left(Z_{rot}^{kin}\right)^{n-1} \exp([(n-1)\tilde{\mu} - U_{n-1}]/k_B T)} = \frac{\rho(Y)}{\rho(X)}. \tag{22}$$

The frequencies of acceptance of new configurations in attempts to change the number of the molecules in the system varied, depending on temperature, within the limits of 0.1–0.5%. For each specific value of n, the random processes 5×10^8 steps long were generated, the first 10^8 steps of which were used for thermalization, and the remaining ones for the calculation of canonical averages.

4. Computer simulation results

4.1. Structure

The patterns of successive growth of condensate nuclei on the defect-free base face of β-AgI crystal and on the nanostructured surface containing periodically repeated defects in the form of rectangular towers from water vapor at a temperature of 260 K are represented in Figs. 1 and 2, respectively. It was observed in preliminary calculations that the adsorption ability of the surface depends crucially on the type of ions present in the surface layer. Stronger adsorption ability is shown by the face, where the first crystallographic layer is formed by Ag^+ ions. This case is represented in Figs. 1 and 2, and for this case all thermodynamic data are calculated in this study. In both cases, on smooth and nanostructured surfaces, surface density of water molecules on the substrate increases with increasing vapor pressure and decreases reversibly with its reduction.

At the same time, molecular mechanisms of the condensate retention on smooth and nanostructured surfaces are qualitatively different. On a smooth surface, see Fig. 1, a successive growth of monomolecular film spots with pronounced hexagonal structure is observed. The spots grow and merge, Fig. 1(a,b), forming a continuous film, as it is seen in Fig. 1(c). The growth of the next layers begins only after the completion of its formation. The molecules in the film form a two-dimensional network resembling the honeycomb structure. Hexagonal molecular cycles are located around the silver cations of the surface layer. The molecules of the cycles are retained on the surface due to the interactions of their hydrogen atoms with the three iodine ions of the second crystallographic substrate layer: hydrogen atoms penetrate deep into the crystal lattice and establish hydrogen bonds with iodine ions. In these conditions, the interaction of the molecules with silver cations is not consolidating one, but has a loosening character – the energy

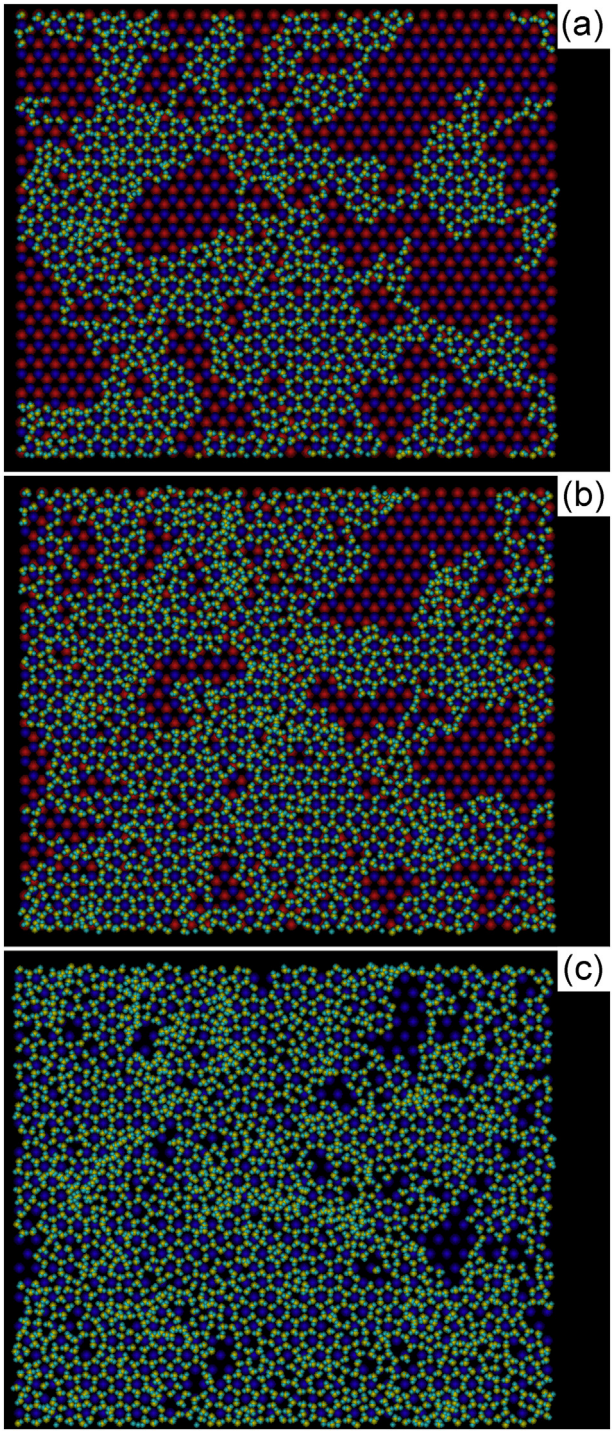

Fig. 1. The growth of the molecular film on the basal face of the β-AgI crystal with Ag^+ ions in the surface crystallographic layer, without surface defects, at a temperature of 260 K. A periodic cell of a size of 32×32 ions with different numbers of molecules is depicted: $N =$ 1224 (a), 1621 (b) and 2152 (c). The last figure shows only Ag^+ ions of the surface crystallographic layer. Blue (dark) color indicates Ag^+, and red (light) color indicates I^- ions.

of interaction with these ions has a positive sign which corresponds to the repulsion. Six more hydrogen atoms are involved in integrity of the hexagonal cycles, and the remaining three atoms are involved in interactions with neighboring atoms. Thermal fluctuations introduce disturbances into this picture which consist mostly in spontaneous redistributions of hydrogen atoms between molecule-molecule and molecule-ions interactions.

A deficiency of free hydrogen atoms in such a structure is a main cause of the hydrophobicity of the film and inhibition of its growth in the direction perpendicular to adsorbing surface. The hydrophobicity of the film is confirmed also by an oscillating character of free energy on β-AgI surface [55,65]. In [66], a long-living state of nonspreading microdroplet on the surface of water monomolecular film adsorbed on a crystalline substrate with a similar hexagonal structure was reproduced by molecular dynamics method.

A qualitatively different picture of the adsorption of vapor molecules is observed on nanostructured surface, as it can be seen in Fig. 2. The monomolecular film with the hexagonal structure does not form here. Instead, water molecules are captured one by one in the most favorable places of the crystal structure and kept there solely due to direct interactions with the ions of crystal lattice. Although a weak tendency of the formation of molecular chains on two opposite lateral faces is observed, Fig. 2(a,d), intermolecular interactions are not a decisive factor in the retention of molecules at this stage.

Under extremely low vapor pressures above the substrate (0.2×10^{-3} Pa, which is 10^{-6} of saturation pressure at this temperature), the first molecules are captured by the lateral faces of the defects, Fig. 2(a–c). At this stage, the upper edge of the defect and the supporting surface of the crystal between the defects remain free of molecules, Fig. 2(a–c). After increasing the vapor pressure, some molecules begin to settle on the upper face of the defect, Fig. 2(d), and then cover it completely, Fig. 2(e). The molecules appear on the surface between the defects only after the "tower" turns out to be covered with a continuous layer of molecules, Fig. 2(f).

The main difference in the mechanisms of the adsorption of water molecules on smooth and structured AgI surfaces is high degree of clusterization of molecules which accompanies the adsorption on ideal surface and is absent on nanostructured one. The growth of two-dimensional film spots on ideal crystal surface is like the nucleation of a two-dimensional gas and can be described in spirit of classic nucleation theory. In contrast, when condensing on nanostructured surface, the role of strongly non-uniform substrate field turns out to be decisive. In this case, collective effects inside the growing nuclei are weakened at the background of the substrate field.

Heating from the temperature, below the freezing point to a value exceeding the boiling point of water does not lead to cardinal changes in the molecular mechanisms of the retention on the surface. Under high temperature, defects still remain active centers of nucleation. With increase of the vapor pressure, they get coated with molecules long before the filling of the space between defects begins. At the temperature of 400 K, like that at 260 K, the capture of vapor molecules occurs first on the side faces of the defects (see Fig. 3(a,b)), although the tendency of the formation of chain structures here is weakened. With increasing vapor pressure, the molecules cover first the top face of the defect, Fig. 3(c–d), and only then settle on the carrier surface between the defects, Fig. 3(e). The elevated temperature makes adsorption on the upper face of the defect more probable than on the supporting surface between the defects, Figs. 2(f) and 3(f). This is an indication of somewhat higher entropy of molecules on upper face.

4.2. Free energy and enthalpy of attachment reaction

The Gibbs free energy, Fig. 4(a), and the enthalpy, Fig. 4(b), of attachment of water molecules to the adsorbate retained on nanostructured surface grow with the increasing number of adsorbed molecules. Under the conditions of a sufficiently rarefied vapor, $p\,\mathrm{v}_{cond} \ll k_BT$, where v_{cond} is the volume per one molecule in the condensate, the attachment enthalpy is $\Delta H(N,T) = U_{cond}(N,T) - U_{cond}(N-1,T) - p\mathrm{v}_g = \Delta U(N,T) - k_BT$. Here, $\mathrm{v}_g = k_BT/p$ is the volume per one molecule in the water vapor, $\Delta U(N,T) = U_{cond}(N,T) - U_{cond}(N-1,T)$ is the change in the potential part of internal energy of the condensate on the surface due to the attachment of a single molecule, and attachment Gibbs free

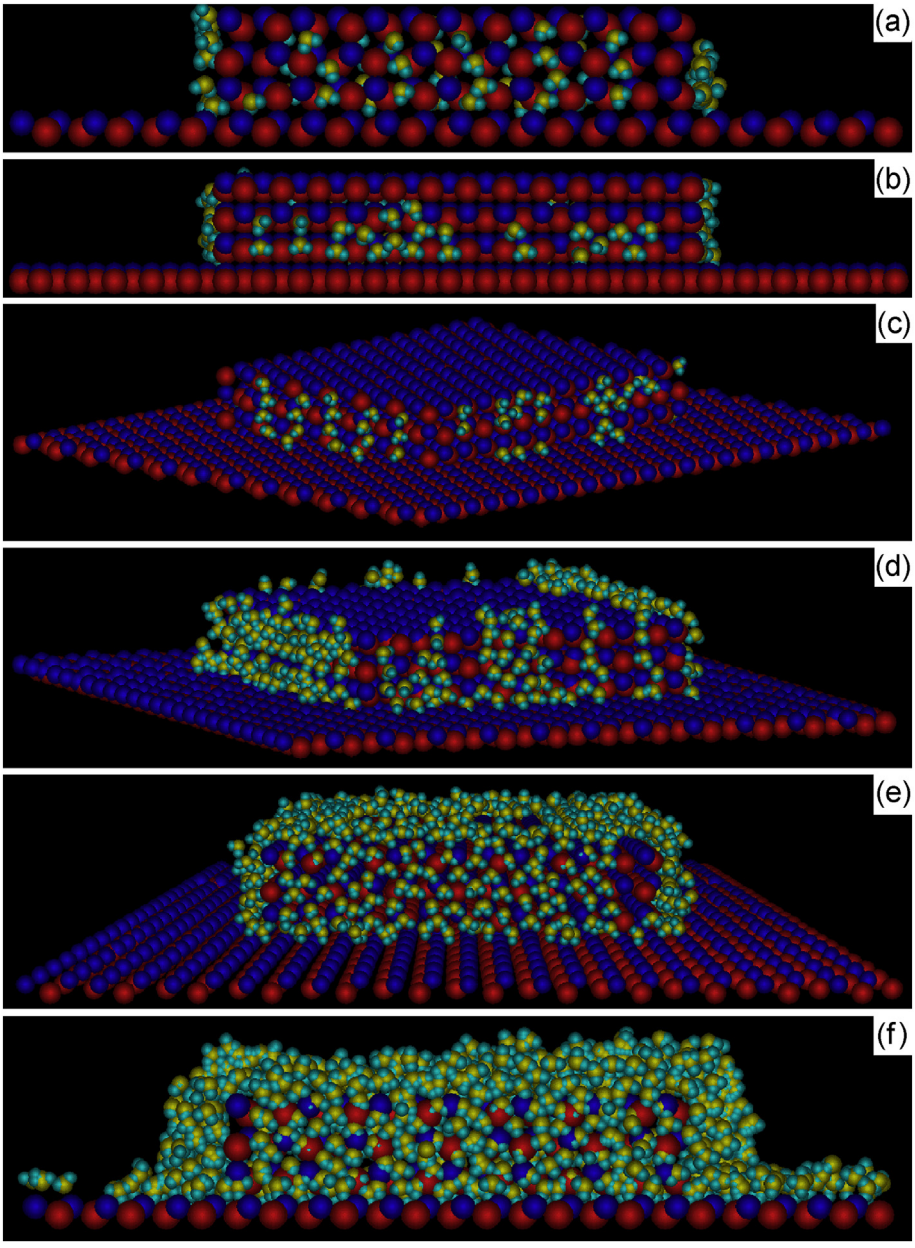

Fig. 2. Sequential precipitation of water vapor molecules at a temperature of 260 K on a nanoscopic fragment in the form of a rectangular "tower" six crystallographic layers in height (three layers of Ag + ions and three layers of I-ions) and with a base of 13 × 13 ions which represents a part of the periodic structure on the surface parallel to the basal face of β-AgI crystal. The stages with different numbers of molecules in periodic cell of the size of 24 × 24 ions are shown: $N = 83$ (a, b, c), 307 (d), 701 (e) и 1224 (f).

energy is $\Delta G(N,p,T) = \mu_{cond}(N,T) - \mu(p,T)$, where $\mu_{cond}(N,T)$ is chemical potential of the molecules in the condensate which is numerically calculated by MBSE method, and $\mu(p,T)$ is vapor molecules chemical potential for which the formula of ideal gas of rigid rotators is applied. The increase in the enthalpy in Fig. 4(b) is due to a stronger interaction of molecules with the substrate than with neighboring molecules. This energy factor is also the main reason for the growth of free energy in Fig. 4(a). This effect is amplified in free energy also due to the entropy drop, Fig. 5(a), (curve 2), which reflects strengthening the rigidity of molecular structure in the conditions of nanostructured surface. The entropy is contained in free energy with negative sign, −TS, so the drop of the entropy contributes to the growth of free energy. The role of crystal lattice field turns out here to be the leading one. Against the background of highly nonuniform field above the substrate with surface defects, collective effects, in particular, the degree of clusterization of the molecules adsorbed on the surface is also weakened. Thus, both the energy and entropy factors make their commensurate contributions into the growth of attachment free energy here, which also persists with increasing temperature, see curve 2 in Fig. 4(a).

The growth of attachment free energy $\Delta G(N,p,T)$ means the positive signs of the second derivatives of Gibbs free energy $G_{cond}(N,T) = \sum_{n=1}^{n=N} \mu_{cond}(n,T)$ and of the formation work of the condensate on the surface

$$A(N,p,T) = G_{cond}(N,T) - N\mu(p,T) \tag{23}$$

as functions of the number of adsorbed molecules: $\frac{\partial^2 A(N,p,T)}{\partial N^2} = \frac{\partial^2 G_{cond}(N,p,T)}{\partial N^2} = \frac{\partial \mu_{cond}(N,T)}{\partial N} > 0$. In turn, the positivity of the second derivative of the formation work at the equilibrium point with the vapor $\mu_{cond}(N,T) = \mu(p,T)$, $\frac{\partial A(N,p,T)}{\partial N} = 0$, means the existence of a minimum on the dependence (23) and thermodynamic stability of the state. Thus, the growing dependence of attachment free energy in Fig. 4(a) entails thermodynamic stability of the condensate which persists also even at elevated

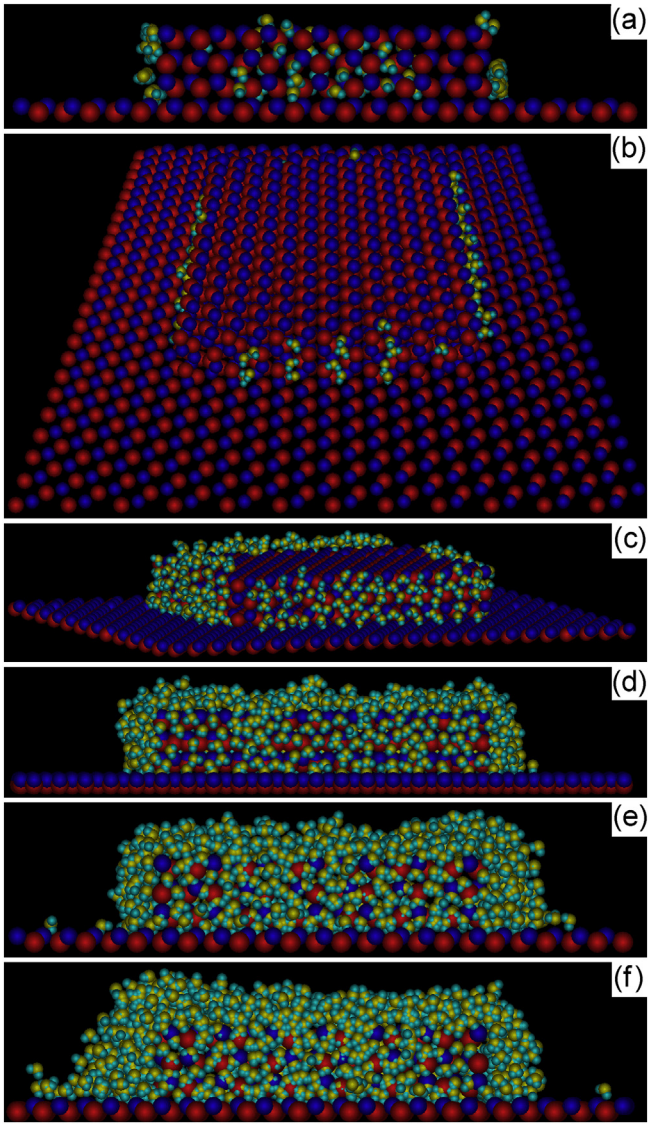

Fig. 3. The same as in Fig. 1, at a temperature of 400 K, and with different numbers of the molecules per periodic cell: N = 83 (a,b), 307 (c), 701 (d), 925 (e) и 1224 (f).

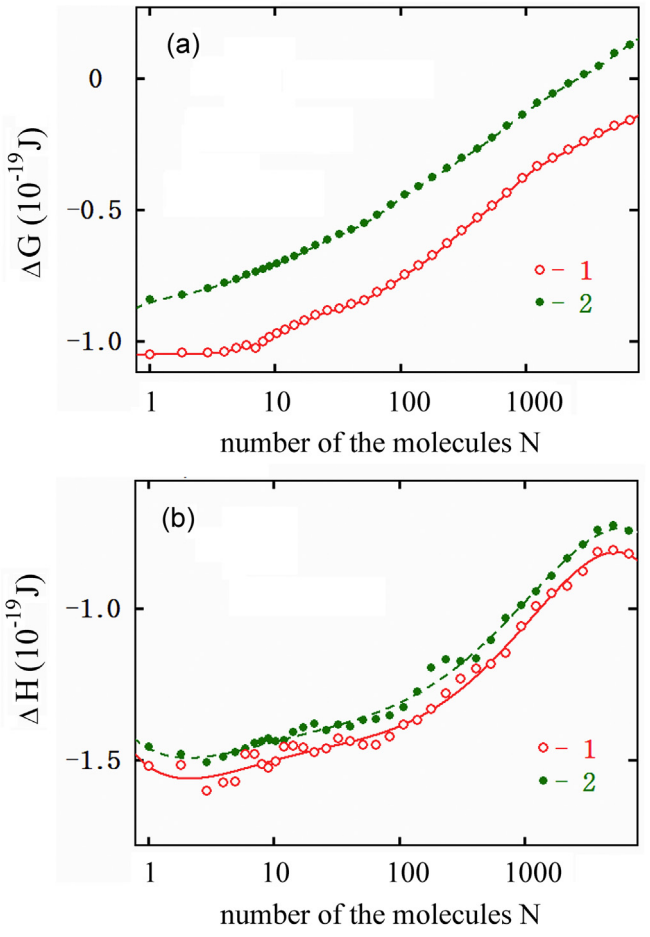

Fig. 4. The free energy (a) referred to the standard vapor pressure of 1 atm. and the enthalpy (b) of the attachment of water vapor molecule to the nanostructured crystal surface shown in Figs. 2,3, depending on the number of the molecules per one periodic cell 24 × 24 ions in size at temperatures of 260 K (curve 1) and 400 K (curve 2).

temperatures. On a smooth adsorption surface, the dependence of formation work on the surface density of the condensate has a more complex shape, due to layer-by-layer adsorption and edge effects as a result of the formation of film spots [55].

The total energy of the condensate in the model of rigid rotators in the system with fixed lattice ions is equal to $E_{cond}(N,T) = U_{cond}(N,T) + (6N/2)k_BT$, and the enthalpy is $H_{cond}(N,p,T) = E_{cond}(N,T) + Npv_{cond}$. In sufficiently rarefied vapors, $pv_{cond} \ll k_BT$, the difference between the enthalpy and the internal energy of the condensate can be neglected, and the dependence on the pressure in the enthalpy is absent: $H_{cond}(N,p,T) \approx E_{cond}(N,T) = H_{cond}(N,T)$. The entropy of the condensate in these conditions does not depend on the pressure above the surface, as well: $S_{cond}(N,T) = (H_{cond}(N,T) - G_{cond}(N,T))/T$.

4.3. Entropy

Fig. 5(a) shows the calculated dependences of the specific entropy of the adsorbed component on the smooth (curve 1) and nanostructured (curve 2) crystal surfaces as a function of the amount of adsorbed material. With the increase of adsorption density, the entropy monotonically decreases with approximately the same rate for both kinds of surfaces. The absolute values of the entropy on the nanostructured surface are lower than that on the smooth surface, which indicates more rigid bonds with the substrate in the presence of defects. The curves of entropy, drawn on a linear scale, first show a sharp drop, and then a shallower course, Fig. 5(b). The sharp change in slope on curve 1 in the region of $N = 6$ corresponding to the smooth surface of adsorption reflects the formation of a closed six-member molecular cycle. A six-member ring fits poorly into the structure of the electric field of the nanostructured substrate, and the same feature in the form of the curve 2 at $N = 6$ is absent. Instead of a six-member cycle, a relatively strong structural element here is a molecular dimer. This is evidenced by a sharp drop in entropy on curve 2, accompanying the attachment of the second molecule, and its relatively smooth course for the next molecules. It should be noted that a rigid design that corresponds to low entropy, under conditions of thermal fluctuations, is not necessarily the most stable. Since the entropy term $-TS$ is contained in free energy with the opposite sign, a decrease in entropy does not mean a decrease in free energy, but quite the contrary. Analysis of the behavior of free energy shows that, on the defect-free surface, at the initial stage of the condensation, five-member cycles successfully compete with six-member ones. The hexagonal structure acquires stability only after the formation of a network of hydrogen bonds and is, therefore, the result of collective effects.

4.4. Formation work

To obtain the dependences of the work of adsorption of water vapors at different pressures, it is sufficient to calculate once the dependence of

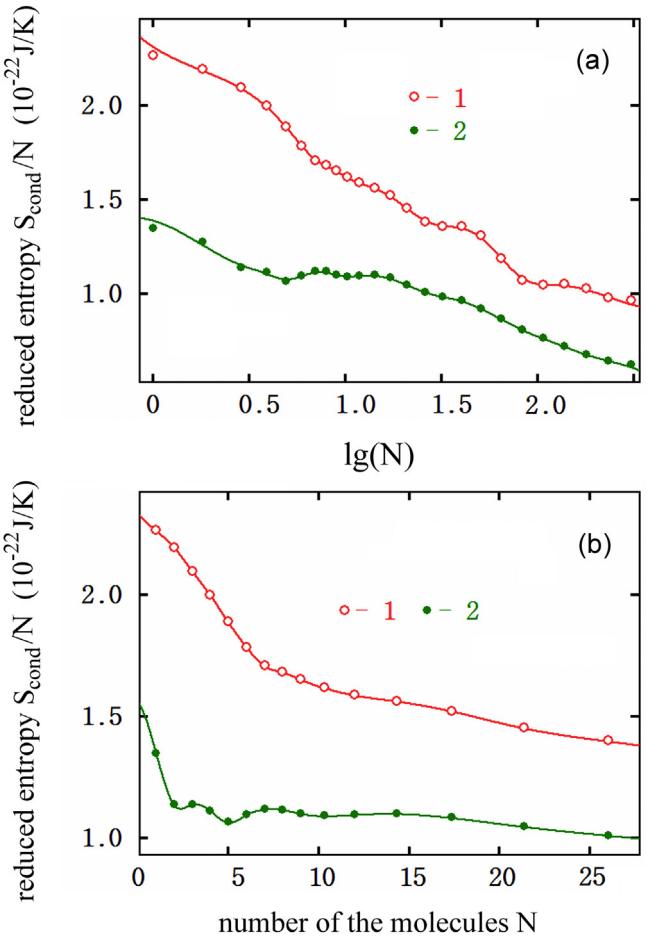

Fig. 5. The entropy of the condensate (calculated per molecule) on smooth, as in Fig. 1 (curves 1) and nanostructured, as in Figs. 2,3 (curves 2) crystal surfaces at a temperature of 260 K, depending on the number of the molecules within the periodic cell: a – in the range of moderate values of surface density, b – in the region of low densities (linear scale).

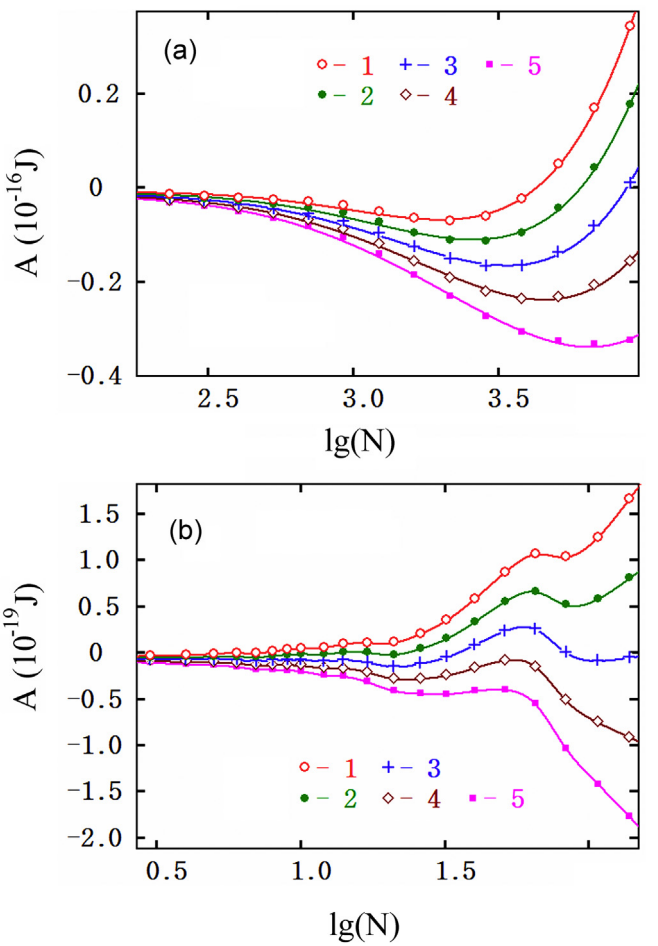

Fig. 6. The equilibrium work of water molecules attachment per one periodic cell to smooth crystal surface shown in Fig. 1, at a temperature of 260 K of water vapors at different pressures close to and higher than saturation value: 1–156, 2–262, 3–441, 4–742, 5–1247 Pa (a). The same for strongly unsaturated vapors: 1–23.2, 2–27.6, 3–32.8, 4–39.0, 5–46.3 Pa (b).

free energy $G_{cond}(N,T)$ on N, which must then be substituted into Eq. (23) using the expression for chemical potential of vapor molecules in the approximation of an ideal gas of rigid rotators.

$$\mu(p,T) = -k_B T \ln\left(\frac{8\pi^2}{\sigma}\frac{k_B T}{p} Z_{tr}^{kin} Z_{rot}^{kin}\right). \quad (24)$$

Thus, the entire dependence on pressure in the right-hand side of Eq. (23) reduces to the logarithmic function $A(N,p,T) = -Nk_BT \ln(p/k_BT) + \ldots$ in the summand linear in N. Although the masses, moments of inertia, and symmetry parameter of the molecules are present in the expression (24), the work of the formation of condensed phase embryo $A(N,p,T)$ does not depend on them, since the same terms, but with the opposite sign are contained also in $G_{cond}(N,T)$ and cancel out in the expression (23).

Fig. 6 shows the dependences of the work of the formation from the vapor at different pressures on the smooth (defect-free) crystal surface, and in Fig. 7, the results of comparative calculations for smooth and nanostructured surfaces are presented. Fig. 6(a) shows the dependences in the region of the medium surface densities, and in Fig. 6(b), corresponding dependences in the region of low density are depicted. An ideal monomolecular film corresponds to $N = 2048$ molecules within the periodic cell or the surface density of 0.11 Å^{-2}. The saturated vapor pressure over a flat interface at 260 K is 200 Pa: curve 1 in Fig. 6 (a) corresponds to unsaturated vapor, and curves 4–6 are obtained for supersaturated vapor.

The minimum representing the stable thermodynamic equilibrium on curve 1 is located in the region of $N = 1800$ i.e., it corresponds to a state of an incompletely filled monomolecular film. The minimum on curve 2 corresponding to a slightly supersaturated vapor is located in the region of $N = 2500$ which is somewhat larger than in the state with the completely filled monomolecular film. Between these curves, there are the states corresponding to saturated vapor with the minimum on the curve of adsorption work close to the state of completely filled monomolecular film. Thus, for saturated water vapor at 260 K, the base face of the crystal is completely covered with the monomolecular film.

The equilibrium between the film and the vapor is stable - with increasing vapor pressure the thickness of the film grows successively, and as the pressure decreases, some of the molecules reversibly evaporate causing ruptures in the continuous film. In the region of highly unsaturated vapor, at the pressures several times lower than saturation, and the surface densities 1–2 orders of magnitude smaller than in the monomolecular film, the adsorption curves have a more complex shape, with local maximums corresponding to an unstable equilibrium with the vapor, Fig. 6(b). The maximums of the adsorption curves are due to a specific nucleation regime at this stage: the molecules are organized here into flat clusters and monomolecular film spots with excess positive free energy at their edges. The edges of these spots produce the same effect as the surface free energy of the embryos in the homogeneous nucleation of bulk gases, forming a complex shape of the free energy curves and the maximums on the curves of formation work

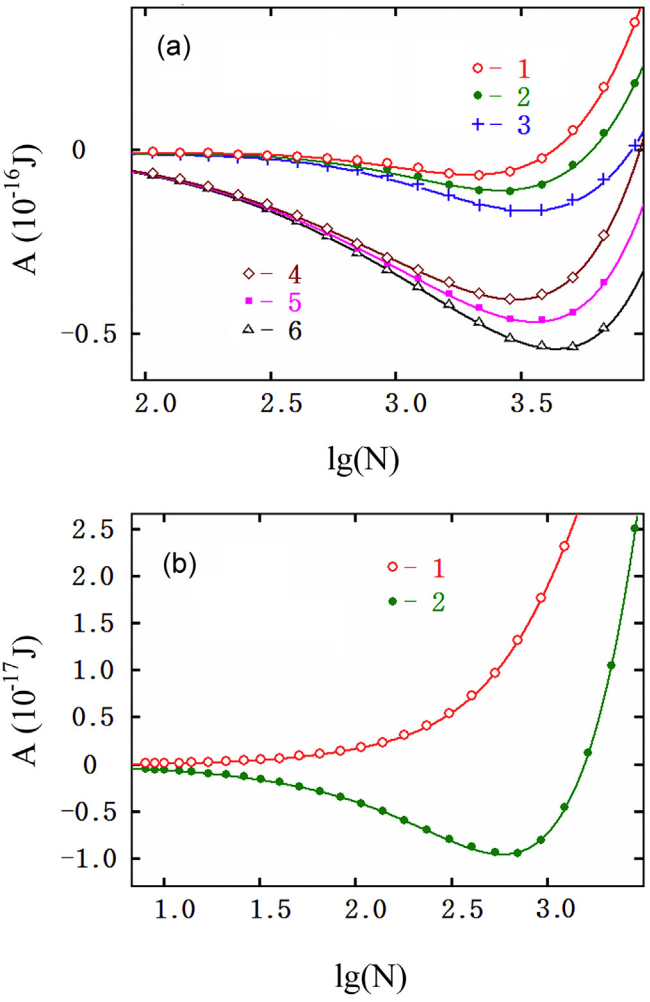

Fig. 7. The equilibrium work of water molecules attachment to smooth crystal surface shown in Fig. 1 (curves 1, 2, 3) and nanostructured surface depicted in Figs. 2,3 (curves 4, 5, 6) per one periodic cell at a temperature of 260 K, at different vapor pressures *p*: a - 156 (1,4), 262 (2,5) and 441 (3,6) Pa; b - 0.256 (1,2) Pa.

[55]. At the same time, the maximums on the curves in Fig. 6(b) are too low to noticeably inhibit the adsorption with the formation of metastable states (note the scales along the vertical axis in Fig. 6(a) and (b)). However, the oscillating shape of the curves influences the equilibrium size distribution of the clusters.

Fig. 7 shows the results of comparative calculations of the formation work at the same vapor pressures on the smooth and nanostructured surfaces of β-AgI crystal. Fig. 7(a) depicts the curves obtained at pressures somewhat lower (curves 1 and 4) and much higher (curves 2,3,5,6) than saturation pressure, and in Fig. 7(b), the results for extremely low pressures are presented. Comparison of the dependences presented in Fig. 7(a) shows that surface nanostructuring leads to a strengthening of adhesion of the adsorbate to the substrate and a decrease in adsorption work. In saturated vapor, the equilibrium amount of adsorbed material in the case of the nanostructured surface, other things being equal, is approximately 20–25% greater than on smooth crystal surface. Under conditions of extremely low vapor pressure, Fig. 7(b), this difference can increase by an order of magnitude and even more.

Fig. 7(b) shows the results for a pressure at which there are no molecules on a smooth surface in the equilibrium state, and, at the same time, several hundred molecules per periodic cell are retained on the nanostructured surface. Thus, the enhanced adsorption capacity of the nanostructured surface shows itself the stronger, the lower the vapor pressure above the substrate. In the stability region of a completely filled monomolecular film, the nanostructured surface retains about one-quarter of the molecules more than the smooth crystal surface. In supersaturated vapors, this difference is leveled gradually with increasing pressure.

The dependences of formation work depicted in Fig. 8 give an idea of the effect of temperature on the adsorption capacity of the nanostructured surface: the curves at 260 K for unsaturated pressures and at 400 K for approximately two thousand times higher pressures are close in shape and the depth of the minimums expressed in k_BT units. The increase in temperature from the freezing point to the boiling point of water with simultaneous increase in pressure by more than three orders of magnitude leaves the amount of adsorbed material and its stability on the surface unchanged. The condensed phase embryo rising on the crystal surface is sufficiently stable with respect to temperature variations.

4.5. Thermodynamic stability

An informative characteristic of thermodynamic stability of a condensate embryo on a substrate is the work of its formation from the vapor that is in equilibrium with the embryo:

$$A^{eq}(N,T) = G_{cond}(N,T) - N\frac{\partial G_{cond}(N,T)}{\partial N}. \quad (25)$$

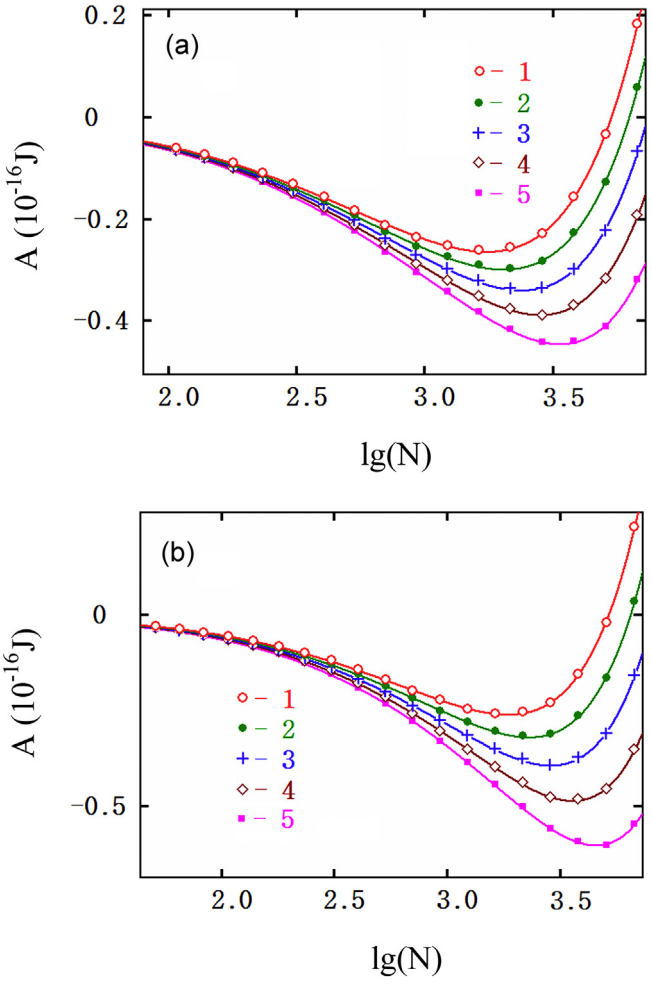

Fig. 8. The equilibrium work of water molecules attachment to the nanostructured surface shown in Figs. 2,3 per one periodic cell in unsaturated vapor, at different pressures *p*: 1–27.6, 2–46.3, 3–77.9, 4–131, 5–220 Pa at $T = 260$ K (a) and 1–47.5, 2–79.8, 3–134, 4–225, 5–379 kPa at $T = 400$ K (b).

The expression (25) is obtained by the substitution of the condition of material balance between the vapor and the condensate

$$\mu(p,T) = \mu_{cond}(N,T) = \frac{\partial G_{cond}(N,T)}{\partial N} \tag{26}$$

into Eq. (23).

The direction of change of $A^{eq}(N,T)$ with variations of N is directly related to the type of extremum (maximum or minimum). Indeed, differentiating expression (25) gives.

$$\frac{\partial A^{eq}(N,T)}{\partial N} = -N\frac{\partial^2 G_{cond}(N,T)}{\partial N^2}. \tag{27}$$

In the case of a maximum ($\frac{\partial^2 G_{cond}(N,T)}{\partial N^2}<0$), the work $A^{eq}(N,T)$ grows with N, whereas in the case of a minimum, on the contrary, it decreases. On the descending part of the curve, the system is thermodynamically stable, and on growing section, is unstable. The sensitivity of this criterion is enhanced at great numbers of molecules by the presence of a factor N in front of the second derivative in the right-hand side of Eq. (27).

The half-width of the minimum on the formation work curve (Eq. (23)) at the point of stable equilibrium is estimated by the quantity

$$\Delta N \approx \left(A^{eq}(N,T)/\frac{\partial^2 G_{cond}(N,T)}{\partial N^2}\right)^{1/2} = N^{1/2}\left(-\frac{\partial \ln\left(|A^{eq}(N,T)|\right)}{\partial N}\right)^{-1/2}. \tag{28}$$

It is seen from Eq. (28), the higher the rate of the fall of $A^{eq}(N,T)$ with N the more acute the minimum on $A(N,p,T)$ curve and the more stable the system at the point of equilibrium. According to the very definition, the quantity $A^{eq}(N,T)$ is equal to the depth of the minimum on the formation work curve $A(n,p,T)$ which at corresponding vapor pressure is located at the point $n = N$. The slope of the $A^{eq}(N,T)$ curve makes it possible to judge about the width of this minimum.

Fig. 9(a) and (b) show the dependences of $A^{eq}(N,T)$ on the number of the molecules per periodic cell calculated in the regions of medium and low values of surface density, respectively. A fast fall of $A^{eq}(N,T)$ means increased stability. It is seen that the stability of the condensate increases with the growth of adsorbed component, and the stabilization occurs earlier on the nanostructured surface. On the smooth surface, the stability sharply increases after the formation of a monomolecular film, whereas the same enhancement of the stability on nanostructured surface takes place at the surface density an order of magnitude lower. The loss of stability (the segment of growing dependence in the region $N \approx 10^3$) is observed at the stage of the fusion of spots into a continuous monomolecular film, Fig. 9(a). At this stage, the edges of the spots are disappearing, and with them, the excess free energy they carry is also annulled. The result is an accelerated drop in the free energy. Following this, the next molecular layer on the surface of the monomolecular film begins to grow. In view of the hydrophobicity of the film surface, the formation of the next layer is coupled with the overcoming of the free energy barrier [55]. The action of the barrier is intensified against the background of accelerated fall of the free energy preceding it. The barrier is a source of thermodynamic instability, and its existence is reflected in the shape of $A^{eq}(N,T)$ curve in form of the growing segment.

In the region of extremely low surface density (see Fig. 9(a)), the stability of adsorbed component on the nanostructured surface is incomparably higher than on smooth crystal surface. This is observed for conditions where the surface density of molecules is insufficient to ensure thermodynamic stability of condensate through collective interactions between molecules. The stability is supported here due to the field of numerous nanostructure elements on the surface. The enhancement of stability is accompanied, according to Eq. (28), by the suppression of fluctuations, producing the effect of "freezing" the adsorbate on the substrate. In combination with entropy data, it should be concluded that on nanostructured surface, the molecules are more rigidly fixed and less mobile than on a smooth crystal surface. This difference between the behavior of the molecules on smooth and nanostructured surfaces is the more pronounced the less the surface density of the molecules.

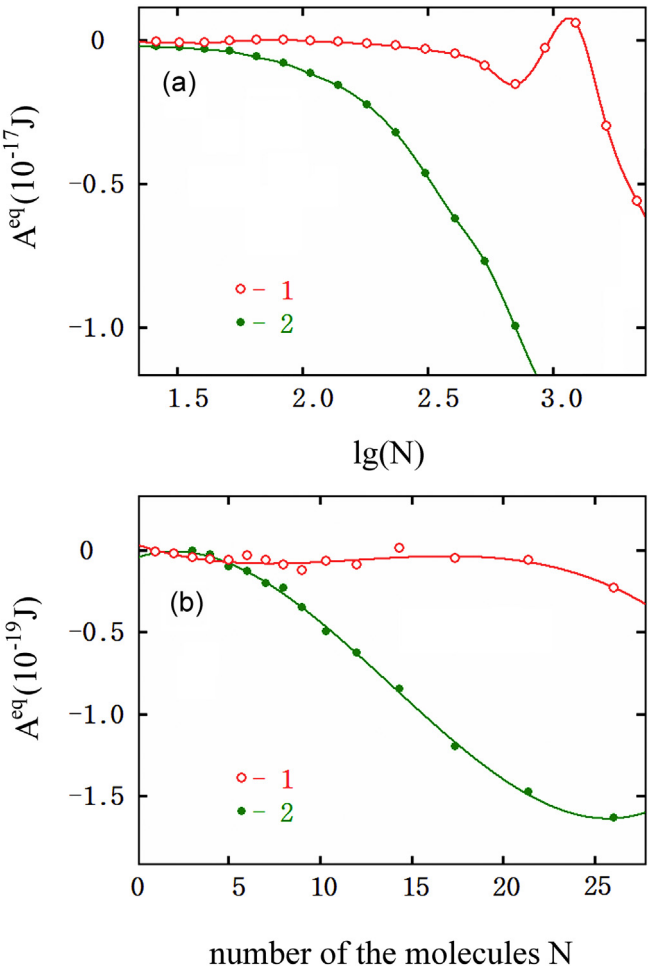

Fig. 9. The work of water molecules attachment to the substrate in the vapor existing in equilibrium with the condensate on smooth (curve 1) and nanostructured (curve 2) surfaces, per one periodic cell at 260 K as functions of the number of molecules within the periodic cell in the regions of moderate (a) and low (b) values of surface densities.

4.6. Adsorption isotherms

Adsorption isotherms (the amount of vapor adsorbed as a function of vapor pressure over the substrate) represent a characteristic that is most often measured in real laboratory experiments and is therefore of particular interest. As it is seen in Fig. 10, the shapes of adsorption isotherms for smooth and nanostructured crystal surfaces are very different. The curve corresponding to nanostructured surface begins in the region of extremely low pressures. The molecules are captured by the surface already at pressures of 10^{-5}–10^{-8} Pa, whereas on smooth surface, the formation of the condensate begins at the pressures 5–6 orders of magnitude higher, Fig. 10(a). Because of the lack of instability effects, which arise due to the formation and fusion of molecular film spots, as is the case on the smooth surface, the isotherm on nanostructured surface is not only strongly extended toward low pressures, but also has a much smoother shape.

The monotonically increasing dependence of the adsorption isotherm is directly related to thermodynamic stability of the condensate.

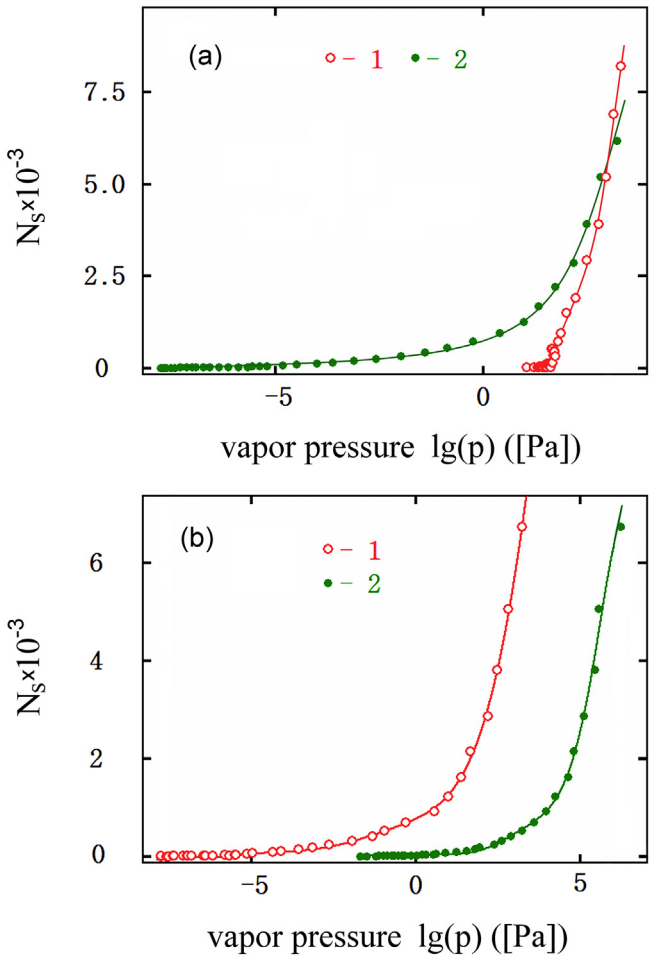

Fig. 10. Isotherms of water adsorption: (a) - equilibrium number of adsorbed vapor molecules per one periodic cell on smooth, as in Fig. 1 (curve 1) and nanostructured, as in Figs. 2,3 (curve 2), surfaces at 260 K; (b) - the same on nanostructured surface at 260 K (curve 1) and at 400 K (curve 2).

Indeed, at the point of equilibrium between the condensate and the vapor$N = N_s$, it follows from the equations

$$\frac{\partial^2 G_{cond}(N,T)}{\partial N^2}\Big|_{N=N_s} = \frac{\partial \mu_{cond}(N,T)}{\partial N}\Big|_{N=N_s} = \frac{\partial \mu(p,T)}{\partial p}\left(\frac{\partial N_s}{\partial p}\right)^{-1} \quad (29)$$

and the expression (24) for chemical potential of vapor molecules $\mu(p,T)$ that

$$\left(\frac{\partial N_s}{\partial p}\right) = \frac{k_B T}{p}\left(\frac{\partial^2 G_{cond}(N,T)}{\partial N^2}\Big|_{N=N_s}\right)^{-1}. \quad (30)$$

In the region of stability, $\frac{\partial^2 G_{cond}(N,T)}{\partial N^2} > 0$, according to Eq. (30), N_s grows with increasing pressure, while in the instability region, on the contrary, it decreases. High thermodynamic stability of the adsorbed component along with a smooth and elongated shape of adsorption isotherm for nanostructured surfaces provide enhanced functional properties of this material for use in programmable adsorption in the conditions of a deep vacuum. Though temperature variations do not change essentially the shape of the adsorption isotherm of nanostructured surface, a significant shift of the curve over pressure is certainly observed. An increase in temperature from the freezing point to the boiling point of water leads to a displacement of the isotherm along pressure axis by 3–4 orders of magnitude (see Fig. 10(b)).

5. Conclusions

In the presented work, the influence of nanoscopic surface topography on the adsorption properties of β-AgI crystal substrate with respect to water vapor is investigated. A concrete type of surface roughness in form of periodically repeating rectangular towers is studied. Unlike previous works, we studied here the more coarse-grained surface, which allows collective effects in the behavior of deposited molecules already in an area comparable to the dimensions of one element of the roughness, and investigated in detail the nucleation of water in its vicinity. In these conditions, it becomes possible to observe different types of structures of adsorbed material on the lateral faces of roughness elements and on their tops.

The main efforts in the present study were focused on obtaining thermodynamic characteristics. The free energy and the entropy as functions of the amount of the material adsorbed are calculated accurately, with the application of simulation methods based on fundamental principles of statistical mechanics. The adsorption properties depend on a specific type of nanostructured surface, and one should not expect that all the quantitative results obtained in this work for a specific case under consideration will also be observed on other surfaces. However, we expect that some of the regularities are fundamental and remain valid for a wide range of surfaces.

A main consequence of nanoscopic surface defects is a sharp increase in thermodynamic stability of the condensate formed on such a surface. The degree of the enhancement of adsorption capacity of the surface depends on the concrete shape and size of roughness elements. The effect of their geometry on the stability of the condensate should be the subject of future research, but even now one can conclude that the relatively coarse-grained relief consisting of convex nanoscopic formations has a significant stimulating effect on the adsorption. The nucleation at such a surface begins in water vapors with the density that is orders of magnitude lower than on a smooth crystal surface and covers a much wider range of pressures. The adsorption isotherm for nanostructured surfaces is much smoother and elongated toward low pressures, which makes it possible to use them as efficient absorber under deep vacuum conditions.

The mechanism of the microcondensation on smooth surfaces differs from that on nanostructured surfaces by a much stronger degree of clustering of molecules. On a structured surface, the clusters are destroyed in a strong electric field of surface inhomogeneities. The adsorption of the water molecules begins at the lateral edges of the nanoscopic structural elements, then continues on their upper faces and lastly extends to the supporting surface between them. The nuclei of the condensed phase formed from the vapor on a smooth surface of the base face of the β-AgI crystal are thermodynamically stable in almost the entire range of vapor pressures. Local stability disturbances can be observed only at the initial stage of the nucleation, when the monomolecular layer is not yet completely filled. On a nanostructured surface, the condensed phase is stable at any pressures, and the presence of nanoscopic inhomogeneity on the surface leads to a significant suppression of fluctuations and the formation of more rigid molecular structure. The amount of water held on the surface increases or decreases reversibly depending on increasing or decreasing pressure. The nanoscopic inhomogeneity of the surface promotes removing free energy barriers and the suppression of metastable states together with hysteresis phenomena in the adsorption-desorption cycle.

The free energy of attachment of water vapor molecules on the basal face of β-AgI crystal with coarse-grained nanoscopic structure is lower than on its smooth surface. The coarse-grained roughness leads to a decrease in both the energy and entropy of the condensate. At the same time, the free energy decreases on the nanostructured surface, since the effect of lowering the internal energy is more pronounced than the opposite effect of decreasing entropy. These features in the thermodynamic behavior of water molecules on a nanostructured surface show

themselves particularly contrastingly at the initial stage of condensation and become stronger with decreasing temperature.

Acknowledgments

This work is supported by The Russian Foundation for Basic Research, RFBR, the project Nos. 17-53-45011-Ind_a, 18-03-00011_a, in part, by the Ministry for Science and Education of the Russian Federation, the project No. 3.4808.2017/6.7 and by the Department of Science & Technology of Indian Government, DST, the project No. INT/RUS/RFBR/P-298.

Appendix A. Summation of long-range electrostatic interactions

In accordance with 2D Ewald method, electrostatic energy of N point charges q_i contained in a periodic cell of the size $l_x \times l_y$ in adsorption plane was written down in form of a two rapidly converging series, over the nodes of the two-dimensional direct and inverse lattices [55]:

$$\begin{aligned} &U(\mathbf{r}_1,\ldots,\mathbf{r}_N) \\ &= \frac{1}{2}\sum_{i=1}^{N}\sum_{j=1}^{N}{\sum_{\mathbf{L}}}' \frac{q_i q_j}{|\,\mathbf{r}_{ij}+\mathbf{L}\,|}\ erfc\,(\alpha|\mathbf{r}_{ij}+\mathbf{L}|) \\ &+\frac{\pi}{2l_x l_y}\sum_{i=1}^{N}\sum_{j=1}^{N}\sum_{\mathbf{H}\neq 0}\frac{q_i q_j}{H}\cos(\mathbf{H}\mathbf{r}_{ij})\left[\ \exp(Hz_{ij})\ erfc\left(\alpha z_{ij}+\left(\frac{H}{2\alpha}\right)\right)\right. \\ &\left.+\exp(-Hz_{ij})\ erfc\left(-\alpha z_{ij}+\left(\frac{H}{2\alpha}\right)\right)\right] \\ &-\frac{\pi}{l_x l_y}\sum_{i=1}^{N}\sum_{j=1}^{N} q_i q_j\left[z_{ij}(1-\ erfc\,(\alpha z_{ij}))+\frac{1}{\alpha\sqrt{\pi}}\exp\left(-\alpha^2 z_{ij}^2\right)\right] \\ &-\frac{\alpha}{\sqrt{\pi}}\sum_{i=1}^{N} q_i^2 \equiv \frac{1}{2}\sum_{i=1}^{N}\sum_{\substack{j=1,\\ j\neq i}}^{N} q_i q_j\varphi\,(\mathbf{r}_{ij})+\sum_{i=1}^{N} q_i^2\xi, \end{aligned} \tag{A1}$$

where $\mathbf{r}_{ij} = (x_{ij}, y_{ij}, z_{ij})$ is the vector connecting the charges q_i and q_j, $\mathbf{L} \equiv (n_x l_x, n_y l_y, 0)$ is a node vector of the lattice in the direct space, and $\mathbf{H} \equiv ((2\pi m_x)/l_x, (2\pi m_y)/l_y, 0)$ is corresponding node vector in inverse space, n_x, n_y, m_x, m_y are integers, α is a parameter determining a concrete way of partition into the sums in direct and inverse spaces, $erfc\,(\ldots)$ is error function. The prime at the sign of the sum in the left-hand side of Eq. (A1) means that for $i = j$, the term with $\mathbf{L} = 0$ is absent there. The last term in the left-hand side owes its existence to the interaction of the charge with its own images. It is obtained as a limiting value at $\mathbf{r} \to 0$ of interaction energy $u_{ii}(\mathbf{r})$ of virtual charge q_i with the same charge and its images in all other cells of the periodicity after the deduction of Coulomb energy of interaction of two charges without taking into account the images:

$$\begin{aligned} u_i^{(s)} = q_i^2 \lim_{\mathbf{r}\to 0}\ \frac{1}{2}\,(\phi\,(\mathbf{r})-1/r) = q_i^2\left\{\frac{\frac{1}{2}\sum_{\mathbf{L}\neq 0} erfc\,(\alpha L)}{L}+\right. \\ \left.+\frac{\pi}{l_x l_y}\left(\sum_{\mathbf{H}\neq 0}\frac{erfc\,(H/(2\alpha))}{H}-\frac{1}{\alpha\sqrt{\pi}}\right)-\frac{\alpha}{\sqrt{\pi}}\right\}. \end{aligned} \tag{A2}$$

The last term in Eq. (A2) is obtained as a limiting value of the difference between the terms with $\mathbf{L} = 0$ in Eq. (A2) and q_i^2/r:

$$\lim_{r\to 0}\ \frac{1}{r}\,[\ erfc\ (\alpha r)-1] = -\frac{2\alpha}{\sqrt{\pi}}. \tag{A3}$$

According to Eq. (A1), the energy of an i-th point charge located at the point $\mathbf{r}_i$ as a part of a molecule has the form:

$$U_i(\mathbf{r}_i) = u_i^{(p)}(\mathbf{r}_i) + u_i^{(s)}, \tag{A4}$$

were $u_i^{(s)} \equiv q_i^2\xi$, $u_i^{(p)}(\mathbf{r}_i) \equiv \sum_{\substack{j=1,\\ j\neq i}}^{N} u_{ij}(\mathbf{r}_{ij})$, and the energy of interaction of i-th charge with other j-th charge at the relative position $\mathbf{r}$ and with its images is

$$u_{ij}(\mathbf{r}) \equiv q_i q_j \varphi\,(\mathbf{r}). \tag{A5}$$

The total energy of the system per one periodic cell in terms of Eq. (A4) has the form

$$U(\mathbf{r}_1,\ldots,\mathbf{r}_N) = \sum_{i=1}^{N}\left(\frac{1}{2}u_i^{(p)}(\mathbf{r}_i)+u_i^{(s)}\right). \tag{A6}$$

The electrostatic energy of a molecule was written as

$$W_n(\mathbf{X}_n,\Omega_n) = w^{(p)}(\mathbf{X}_n,\Omega_n) + w^{(s)}(\Omega_n), \tag{A7}$$

were $\mathbf{X}_n$ and Ω_n are positional and angle coordinates of m-th molecule

$$\begin{aligned} w^{(p)}(\mathbf{X}_n,\Omega_n) &\equiv \sum_{m=1}^{M}{}'\, w(\mathbf{X}_n,\Omega_n;\mathbf{X}_m,\Omega_m) \\ &= \sum_{m=1}^{M}{}'\sum_{l=1}^{P}\sum_{k=1}^{P} u_{lk}(x_{lk}^{nm}) \end{aligned} \tag{A8}$$

has a meaning of the interaction of the molecule with all other molecules within its own periodic cell and their images in all other cells, $\mathbf{x}_{lk}^{nm} = \mathbf{x}_k^m - \mathbf{x}_l^n$ is the vector connecting l-th point charge of n-th molecule and k-th point charge (or its image) of m-th molecule, located within the own periodic cell of l-th point charge of n-th molecule, and

$$w^{(s)}(\Omega_n) \equiv \sum_{l=1}^{P}\left(\frac{1}{2}\sum_{k=1}^{P}{}'\left(u_{lk}(x_{lk}^{nn})-\frac{q_l q_k}{r_{lk}^{nn}}\right)+u_l^{(s)}\right) \tag{A9}$$

is the interaction of the molecule with its own images.

In a general case, the electric field of each molecule is approximated by the field of P point charges. The number of the molecules within the periodic cell in these formulae is equal to M. The strokes at the sum signs mean that the terms with $m = n$ in Eq. (A8) and $k = l$ in Eq. (A9) are absent there. The total energy of electrostatic interaction of the molecules per one periodic cell is equal to

$$W(\mathbf{X}_1,\Omega_1,\mathbf{X}_2,\Omega_2,\ldots,\mathbf{X}_M,\Omega_M) = \sum_{n=1}^{M}\left(\frac{1}{2}w^{(p)}(\mathbf{X}_n,\Omega_n)+w^{(s)}(\Omega_n)\right). \tag{A10}$$

The function $erfc(x)$ was tabulated beforehand, and its values were obtained by interpolating. One-dimensional table saved in the computer's RAM contained 3×10^5 values with the increment of $\Delta x = 10^{-4}$. For a numerical calculation of $u_{ij}(\mathbf{r})$ in Eq. (A4), the values of the function $T(\mathbf{r}; l_x, l_y, \alpha) = \varphi(\mathbf{r}) - 1/r$ within the limits of $0 < x < (1/2)\,l_x$, $0 < y < (1/2)\,l_y$, $0 < z < z_{max}$, at a given values of l_x, l_y and α were also stored in the computer's RAM in the form of three-dimensional table $200 \times 200 \times 400$ in size. The $\varphi(\mathbf{r})$ values were obtained by interpolating table data with account of the parity of the function. At $|z| > z_{max} = Max\ (l_x, l_y)$, the formula for the field of uniformly charged plane $\varphi(\mathbf{r}) = \varphi(x,y,z_{max}) - (2\pi/(l_x l_y))\,(|z| - z_{max})$ was applied.

The same formulae are valid for the calculation of long-range interactions of the molecules with lattice ions within periodic cell having the size $l'_x \times l'_y$ and reduced energy function $\varphi'(\mathbf{r})$ corresponding to them.

Appendix B. Summation of polarization interactions

Two-dimensional version of Ewald method was applied also for the calculation of polarization energy in the field of lattice ions located beyond the own periodic cells of the molecules. The polarization energy was calculated as $w_i^{(pol)} = -\alpha_w E^2(\mathbf{X}_i)/2$, where $E(\mathbf{X}_i) = \mid \mathbf{E}(\mathbf{X}_i) \mid$ is the strength of lattice ions electric field at the center of the i-th molecule. The components of the electric field strength vector at the point $\mathbf{X}$ were calculated by differentiating the reduced energy in the form of the Ewald sum Eq. (A5):

$$\mathbf{E}(\mathbf{X}) = -\sum_{i=1}^{N} q_i \frac{\partial \varphi'(\mathbf{r}_{i0})}{\partial \mathbf{r}_{i0}}, \tag{B1}$$

where $\mathbf{r}_{i0} = \mathbf{X} - \mathbf{r}_i$, and $\mathbf{r}_i$ is the position of i-th ion carrying the charge q_i within the own periodic cell of the molecule. The numeric calculation of $\frac{\partial \varphi'(\mathbf{r})}{\partial \mathbf{r}}$ is even more costly than the calculation of $\varphi'(\mathbf{r})$. For this reason, the calculation of $\frac{\partial \varphi'(\mathbf{r})}{\partial \mathbf{r}}$ was performed by numerical differentiating the interpolated values from the $T(\mathbf{r}; l_x', l_y', \alpha) = \varphi'(\mathbf{r}) - 1/r$ table, already prepared for the calculation of electrostatic interactions of molecule permanent charges with the lattice ions and saved in Double Precision format (with the accuracy of 15 decimal digits).

Appendix C. Summation of dispersion interactions

The contribution of dispersion interactions with neighboring cells can reach $0.1 k_B T$ per one molecule. Relatively rapid decrease of dispersion interaction with the distance ($\sim 1/r^6$) allows restricting the direct summation of these interactions by several closest layers of periodic cells. In the calculations presented, the dispersion interactions with lattice ions were summed up within six layers of periodic cells around the own cell of the molecule. Exchange and dispersion energies of interaction of a single molecule with the crystal were calculated as the sum over the periodic cells

$$U^{DE}(\mathbf{X}, \Omega) = \sum_{n_x=-n_{\max}}^{n_x=n_{\max}} \sum_{n_y=-n_{\max}}^{n_y=n_{\max}} \sum_{i=1}^{I} u_i^{DE}(\mathbf{X}, \Omega, \mathbf{X}_i' + \mathbf{L}', \Omega_i'), \tag{C1}$$

where I is the number of the ions within the periodic cell of the size $l_x' \times l_y'$, $u_i^{DE}(\mathbf{X}, \Omega, \mathbf{X}_i', \Omega_i')$ is exchange and dispersion energy of the interaction of the molecule with the ion, $\mathbf{X}$, Ω are the coordinates of the molecule and $\mathbf{X}_i', \Omega_i'$ are the coordinates of the i-th ion in the own periodic cell of the molecule, and the vector of the cell $\mathbf{L}' = (n_x l_x', n_y l_y', 0)$. The integer $n_{\max}$ determines the number of nearest layers of periodic cells, for which the dispersion interaction with the ions is taken into account.

The sum of exchange and dispersion interactions with the i-th ion located at the point with the coordinates $\mathbf{X}' + \mathbf{L}'$, Ω' has the form

$$u_i^{DE}(\mathbf{X}, \Omega, \mathbf{X}' + \mathbf{L}', \Omega') = \sum_{l=1}^{K} \sum_{k=1}^{K_i} 4\varepsilon_{lk}^i \left(\left(\frac{\sigma_{lk}^i}{|\mathbf{r}_{lk}^i + \mathbf{L}'|} \right)^{12} - \left(\frac{\sigma_{lk}^i}{|\mathbf{r}_{lk}^i + \mathbf{L}'|} \right)^{6} \right), \tag{C2}$$

where ε_{lk}^i and σ_{lk}^i are the parameters of LD potential, $\mathbf{r}_{lk}^i = \mathbf{r}_k^i - \mathbf{r}_l$ is the vector, connecting l-th force center of the molecule and k-th force center (or its image) of the i-th ion, located in the own periodic cell of the l-th center of the molecule, K and K_i are the numbers of force centers of the molecule and of the ion used for the description of exchange and dispersion interactions between the particles.

The values of $T^D(z, l_x', l_y') = U^{DE}(\mathbf{X}, \Omega) - \sum_{i=1}^{I} u_i^{DE}(\mathbf{X}, \Omega, \mathbf{X}_i', \Omega_i')$ at $\mathbf{X} = (0,0,z)$ and $\Omega = (0,0,0)$ as functions of z-coordinate in neglecting the dependence on its x- and y-coordinates as well as on its spatial orientation Ω were calculated, tabulated and stored in computer's RAM before the simulation. First, the one-dimensional table $T^D(z; l_x', l_y')$ 100 elements in size has been constructed by direct numerical summation. Then, the analogous table consisting of 10,000 elements separated by 100 times shorter increments in z was formed with the help of the interpolation of these data by cubic splines. The energy values were extracted from resulting table during the simulation process by linear interpolation.

References

[1] J. Wieringa, I. Holleman, If cannons cannot fight hail, what else? Meteorol. Z. 15 (2006) 659–675.
[2] R. Srivastava, H. Docherty, J.K. Singh, P.T. Cummings, Phase transitions of water in graphite and mica pores, J. Phys. Chem. C 115 (2011) 12448–12457.
[3] R.C. Dutta, S. Khan, J.K. Singh, Wetting transition of water on graphite and boron-nitride surfaces: a molecular dynamics study, Fluid Phase Equilib. 302 (2011) 310–315.
[4] R. Ramírez, J.K. Singh, F. Müller-Plathe, M.C. Böhm, Ice and water droplets on graphite: a comparison of quantum and classical simulations, J. Chem. Phys. 141 (2014), 204701.
[5] R. Benjamin, J. Horbach, Lennard-Jones systems near solid walls: computing interfacial free energies from molecular simulation methods, J. Chem. Phys. 139 (2013), 084705.
[6] U. Terranova, N.H. de Leeuw, Structure and dynamics of water at the mackinawite (001) surface, J. Chem. Phys. 144 (2016) 094706.
[7] J.H. Park, N.R. Aluru, Temperature-dependent wettability on a titanium dioxide surface, Mol. Simul. 35 (2009) 31–37.
[8] W. Xu, Z. Lan, B.L. Peng, R.F. Wen, X.H. Maa, Effect of surface free energies on the heterogeneous nucleation of water droplet: a molecular dynamics simulation approach, J. Chem. Phys. 142 (2015), 054701.
[9] L.S. Pedroza, A. Poissier, M.-V. Fernandez-Serra, Local order of liquid water at metallic electrode surfaces, J. Chem. Phys. 142 (2015), 034706.
[10] K. Kobayashi, Yu. Liang, T. Sakka, T. Matsuoka, Molecular dynamics study of salt–solution interface: solubility and surface charge of salt in water, J. Chem. Phys. 140 (2014), 144705.
[11] M.K. Rana, A. Chandra, Ab initio and classical molecular dynamics studies of the structural and dynamical behavior of water near a hydrophobic graphene sheet, J. Chem. Phys. 138 (2013), 204702.
[12] D. Murakami, K. Yasuoka, Molecular dynamics simulation of quasi-two-dimensional water clusters on ice nucleation protein, J. Chem. Phys. 137 (2012), 054303.
[13] D. Surblys, Y. Yamaguchi, K. Kuroda, T. Nakajima, H. Fujimura, Analysis on wetting and local dynamic properties of single water droplet on a polarized solid surface: a molecular dynamics study, J. Chem. Phys. 135 (2011), 014703.
[14] J.H. Taylor, B.N. Hale, Monte Carlo simulations of water-ice layers on a model silver iodide substrate: a comparison with bulk ice systems, Phys. Rev. B 47 (1993) 9732–9741.
[15] B.N. Hale, J. Kiefer, Studies of H_2O on β-AgI surfaces: an effective pair potential model, J. Chem. Phys. 73 (1980) 923–933.
[16] R.C. Ward, J.M. Holdman, B.N. Hale, Monte Carlo studies of water monolayer clusters on substrates: hexagonal AgI, J. Chem. Phys. 77 (1982) 3198–3202.
[17] R.C. Ward, B.N. Hale, S. Terrazas, A study of the critical cluster size for water monolayer clusters on a model AgI basal substrate, J. Chem. Phys. 78 (1983) 420–423.
[18] G. Fraux, J.P.K. Doye, Note: heterogeneous ice nucleation on silver-iodide-like surfaces, J. Chem. Phys. 141 (2014), 216101.
[19] K. Jug, N.N. Nair, T. Bredow, Molecular dynamics investigation of water adsorption on rutile surfaces, Surf. Sci. 590 (2005) 9–20.
[20] T.A. Ho, D. Argyris, D.V. Papavassiliou, A. Striolo, L.L. Lee, D.R. Cole, Interfacial water on crystalline silica: a comparative molecular dynamics simulation study, Mol. Simul. 37 (2011) 172–195.
[21] A. Reinhardt, J.P.K. Doye, Effects of surface interactions on heterogeneous ice nucleation for a monatomic water model, J. Chem. Phys. 141 (2014), 084501.
[22] K. Raghavan, K. Foster, K. Motakabbir, M. Berkowitz, Structure and dynamics of water at the Pt(111) interface: molecular dynamics study, J. Chem. Phys. 94 (1991) 2110–2117.
[23] O. Pizio, H. Dominguez, L. Pusztai, S. Sokolowski, A core-softened fluid model in disordered porous media. Grand canonical Monte Carlo simulation and integral equations, Phys. A 388 (2009) 2278–2288.
[24] H. Dominguez, A. Patrykiejew, S. Sokolowski, Molecular dynamics study of the formation of small crystallites of Lennard-Jones particles in slit-like pores with (100) fcc walls, Mol. Phys. 101 (2003) 1867–1882.
[25] H. Dominguez, M.P. Allen, R. Evans, Monte Carlo studies of the freezing and condensation transitions of confined fluids, Mol. Phys. 96 (1999) 209–229.
[26] H. Huang, J. Singh, J.M. Lee, S.K. Kwak, Confining effect of carbon nanotube configuration on phase behavior of hard-sphere fluid, Fluid Phase Equilib. 318 (19) (2012) 19–24.
[27] J.K. Singh, S.K. Kwak, Surface tension and vapor-liquid phase coexistence of confined square-well fluid, J. Chem. Phys. 126 (2007), 024702.
[28] S. Jana, J.K. Singh, S.K. Kwak, Vapor-liquid critical and interfacial properties of square-well fluids in slit pores, J. Chem. Phys. 130 (2009), 214707.
[29] V. Velachi, D. Bhandary, J.K. Singh, M.N.D.S. Cordeiro, Striped gold nanoparticles: new insights from molecular dynamics simulations, J. Chem. Phys. 144 (2016), 244710.
[30] D. Bhandary, Z. Benkova, M.N.S. Cordeiro, J.K. Singh, Molecular dynamics study of wetting behavior of grafted thermo-responsive PNIPAAm brushes, Soft Matter 12 (2016) 3093.

[31] M. Svoboda, A. Malijevský, M. Lisal, Wetting properties of molecularly rough surfaces, J. Chem. Phys. 143 (2015), 104701.
[32] R.N. Wenzel, Resistance of solid surfaces to wetting by water, Ind. Eng. Chem. 28 (1936) 988–994.
[33] A. Malijevský, Does surface roughness amplify wetting? J. Chem. Phys. 141 (2014), 184703.
[34] Sh. Chen, J. Wang, T. Ma, D. Chen, Molecular dynamics simulations of wetting behavior of water droplets on polytetrafluorethylene surfaces, J. Chem. Phys. 140 (2014), 114704.
[35] A.K. Metya, S. Khan, J.K. Singh, Wetting transition of the ethanol–water droplet on smooth and textured surfaces, J. Phys. Chem. C 118 (2014) 4113–4121.
[36] J.K. Singh, F. Muller-Plathe, On the characterization of crystallization and ice adhesion on smooth and rough surfaces using molecular dynamics, Appl. Phys. Lett. 104 (2014), 021603.
[37] Yun-Wen Chen, Hai-Ping Cheng, Interaction between water and defective silica surfaces, J. Chem. Phys. 134 (2011), 114703.
[38] L. Lupi, A. Hudait, V. Molinero, Heterogeneous nucleation of ice on carbon surfaces, J. Am. Chem. Soc. 136 (2014) 3156–3164.
[39] F. Hong, Yu H. Ni, W.Ju. Xu, Ya Yan, Origin of enhanced water adsorption at ⟨110⟩ step edge on rutile TiO_2(110) surface, J. Chem. Phys. 137 (2012) 114707.
[40] U. Martinez, L.B. Vilhelmsen, H.H. Kristoffersen, J. Stausholm-Møller, B. Hammer, Steps on rutile TiO_2(110): active sites for water and methanol dissociation, Phys. Rev. B 84 (2011) 205434.
[41] A. Tilocca, A. Selloni, Structure and reactivity of water layers on defect-free and defective anatase TiO_2(101) surfaces, J. Phys. Chem. B 108 (2004) 4743–4751.
[42] A. Tilocca, A. Selloni, Reaction pathway and free energy barrier for defect-induced water dissociation on the (101) surface of TiO_2-anatase, J. Chem. Phys. 119 (2003) 7445–7450.
[43] M. Posternak, A. Baldereschi, B. Delley, Dissociation of water on anatase TiO_2 nanoparticles: the role of undercoordinated Ti atoms at edges, J. Phys. Chem. C 113 (2009) 15862–15867.
[44] X.-Q. Gong, A. Selloni, Role of steps in the reactivity of the anatase TiO_2(101) surface, J. Catal. 249 (2007) 134–139.
[45] M. Cardellach, A. Verdaguer, Two-dimensional wetting: the role of atomic steps on the nucleation of thin water films on BaF2(111) at ambient conditions, J. Chem. Phys. 132 (2010), 234708.
[46] Xi.-Xi. Zhang, M. Chen, M. Fu, Impact of surface nanostructure on ice nucleation, J. Chem. Phys. 141 (2014) 124709.
[47] F. Bottiglione, G. Carbone, B.N.J. Persson, Fluid contact angle on solid surfaces: role of multiscale surface roughness, J. Chem. Phys. 143 (2015), 134705.
[48] A.B.D. Cassie, Contact angles, Discuss. Faraday Soc. 3 (1948) 11–15.
[49] R.N. Wenzel, Surface roughness and contact angle, J. Phys. Chem. 53 (1949) 1466–1467.
[50] K. Koch, B. Bhushan, W. Barthlott, Diversity of structure, morphology and wetting of plant surfaces, Soft Matter 4 (2008) 1943–1963.
[51] J.Y. Yan, G.N. Patey, Ice nucleation by electric surface fields of varying range and geometry, J. Chem. Phys. 139 (2013), 144501.
[52] A.P. Lyubartsev, A.A. Martsinovski, S.V. Shevkunov, P.N. Vorontsov-Velyaminov, New approach to Monte Carlo calculation of the free energy: method of expanded ensembles, J. Chem. Phys. 96 (1992) 1776–1783.
[53] R.W.G.Wyckoff, Crystal Structures, 1, 1965 110 (New York, Intersc.publ).
[54] G. Burley, An x-ray determination of the Debye temperature of silver iodide, J. Phys. Chem. Solids 25 (1964) 629–634.
[55] S.V. Shevkunov, Stimulation of vapor nucleation on perfect and imperfect hexagonal lattice surfaces, J. Exper. Theor. Phys. 107 (2008) 965–983.
[56] S.V. Shevkunov, Numerical simulation of water vapor nucleation on electrically neutral nanoparticles, J. Exper. Theor. Phys. 108 (2009) 447–468.
[57] S.V. Shevkunov, A.A. Martsinovski, P.N. Vorontsov-Velyaminov, Monte Carlo calculation of the critical size and properties of the microdroplets in expanded ensemble, Teplofizika vysokih temperatur 26 (1988) 246–254 (Russian Acagemy of Sciences, in Russian).
[58] S.V. Shevkunov, A.A. Martsmovski, P.N. Vorontsov-Velyammov, A new Monte Carlo method for direct calculation of the critical size and the formation work of microdrop, Mol. Simul. 5 (1990) 119–132.
[59] S.V. Shevkunov, S.I. Lukyanov, J.-M. Leyssale, Cl. Millot, Computer simulation of Cl-hydration in anion-water clusters, Chem. Phys. 310 (2005) 97–107.
[60] S.I. Lukyanov, Z.S. Zidi, S.V. Shevkunov, Ion-water cluster free energy computer simulation using some of most popular ion-water and water-water pair interaction models, Chem. Phys. 332 (2007) 188–202.
[61] S.I. Lukyanov, Z.S. Zidi, S.V. Shevkunov, Monte Carlo bicanonical ensemble simulation for sodium cation hydration free energy in liquid water, Fluid Phase Equilib. 233 (2005) 34–46.
[62] S.V. Shevkunov, Intermolecular interactions and thermophysical properties of clusters and the calculation of free energy of $H_3O + (H_2O)n$ complexes by the Monte Carlo method, Colloid J. 67 (2005) 509–515.
[63] S.V. Shevkunov, Effect of chlorine ions on the stability of nucleation cores in condensing water vapors, Russ. J. Phys. Chemistry A 85 (2011) 1584–1591.
[64] S.V. Shevkunov, The hydrate shell of a Cl–ion in a planar nanopore. Thermodynamic stability, Russ. J. Electrochem. 50 (2014) 1127–1136.
[65] S.V. Shevkunov, Layer-by-layer adsorption of water molecules on the surface of a silver iodide crystal, Russ. J. Phys. Chem. 80 (2006) 769–775.
[66] Ch. Wang, H. Lu, Zh. Wang, P. Xiu, B. Zhou, G. Zuo, R. Wan, J. Hu, H. Fang, Stable liquid water droplet on a water monolayer formed at room temperature on ionic model substrates, Phys. Rev. Lett. 103 (2009), 137801.